

UTILIZATION OF CFD TOOLS IN THE DESIGN PROCESS
OF
A FRANCIS TURBINE

A THESIS SUBMITTED TO
THE GRADUATE SCHOOL OF NATURAL AND APPLIED SCIENCES
OF
MIDDLE EAST TECHNICAL UNIVERSITY

BY

GİZEM OKYAY

IN PARTIAL FULFILLMENT OF THE REQUIREMENTS
FOR
THE DEGREE OF MASTER OF SCIENCE
IN
CIVIL ENGINEERING

SEPTEMBER 2010

Approval of the thesis:
**UTILIZATION OF CFD TOOLS IN THE DESIGN PROCESS OF A
FRANCIS TURBINE**

submitted by **GİZEM OKYAY** in partial fulfillment of the requirements for the degree of **Master of Science in Civil Engineering Department, Middle East Technical University** by,

Prof. Dr. Canan Özgen
Dean, Graduate School of **Natural and Applied Sciences** _____

Prof. Dr. Güney Özcebe
Head of Department, **Civil Engineering** _____

Assoc. Prof. Dr. İsmail Aydın
Supervisor, **Civil Engineering Dept., METU** _____

Prof. Dr. Metin Ger
Co-Supervisor, **Civil Engineering Dept., IKU** _____

Examining Committee Members

Assoc. Prof. Dr. Zafer Bozkuş
Civil Engineering Dept., METU _____

Assoc. Prof. Dr. İsmail Aydın
Supervisor, Civil Engineering Dept., METU _____

Prof. Dr. Metin Ger
Co-Supervisor, Civil Engineering Dept., IKU _____

Asst. Prof. Dr. Selin Aradağ Çelebioğlu
Mechanical Engineering Dept., TOBB ETU _____

Dr. Kutay Çelebioğlu
Civil Engineer, General Manager, SU-ENER _____

Date: _____

I hereby declare that all information in this document has been obtained and presented in accordance with academic rules and ethical conduct. I also declare that, as required by these rules and conduct, I have fully cited and referenced all material and results that are not original to this work.

Name, Last name : Gizem Okyay

Signature :

ABSTRACT

UTILIZATION OF CFD TOOLS IN THE DESIGN PROCESS OF A FRANCIS TURBINE

OKYAY, Gizem

M.Sc., Department of Civil Engineering

Supervisor: Assoc. Prof. Dr. İsmail AYDIN

September 2010, 109 pages

Francis type turbines are commonly used in hydropower generation. Main components of the turbine are spiral case, stay vanes, guide vanes, turbine runner and the draft tube. The dimensions of these parts are dependent mainly on the design discharge, head and the speed of the rotor of the generators. In this study, a methodology is developed for parametric optimization by incorporating Matlab codes developed and commercial Computational Fluid Dynamics (CFD) codes into the design process. The design process starts with the selection of initial dimensions from experience curves, iterates to improve the overall hydraulic efficiency and obtain the detailed description of the final geometry for manufacturing with complete visualization of the computed flow field. A Francis turbine designed by the procedure developed has been manufactured and installed for energy production.

Keywords: Francis turbine, computational fluid dynamics, CFD, turbine design, hydropower

ÖZ

FRANCİS TÜRBİNİ TASARIM SÜRECİNDE HESAPLAMALI AKIŞKANLAR DİNAMİĞİ ARAÇLARININ KULLANILMASI

OKYAY, Gizem

Yüksek Lisans, İnşaat Mühendisliği Bölümü

Tez Danışmanı: Doç. Dr. İsmail AYDIN

Eylül 2010, 109 sayfa

Francis tipi türbinler hidroelektrik enerjisi üretiminde yaygın olarak kullanılmaktadır. Türbinin temel bileşenleri sarmal boru, sabit kanatlar, ayar kanatları, çark kanatları ve emme borusudur. Bu parçaların boyutları tasarım debisine, düşüye ve jeneratörün hızına bağlıdır. Bu çalışmada, parametrik iyileştirme için geliştirilen Matlab kodları ile ticari Hesaplamalı Akışkanlar Mekaniği (CFD) kodlarının tasarım sürecinde etkileşimli kullanılması için bir metod geliştirilmiştir. Tasarım süreci, tecrübe eğrilerinden türbin başlangıç boyutları seçimi ile başlar, genel hidrolik verimliliğin artırılması için denemeler yapılır ve sonuç geometrinin imalat için detaylı bir tanımı, görselleştirilmiş akım alanı ile birlikte elde edilir. Bu yöntemle tasarlanmış bir Francis türbini imal edilmiş ve enerji üretimi için kurulmuştur.

Anahtar Kelimeler: Francis türbini, hesaplamalı akışkanlar dinamiği, HAD, türbin tasarımı, hidroelektrik

*“Faites que le rêve dévore votre vie
afin que la vie ne dévore pas votre rêve.”*

Antoine de Saint-Exupéry

To my beautiful family

ACKNOWLEDGMENTS

I express my sincere appreciation to my supervisors Assoc. Prof. Dr. İsmail Aydın and Prof. Dr. Metin Ger for their guidance, understanding and advice.

I would like to express my deepest gratitude to my manager Dr. Kutay Çelebioğlu for his inspiration, guidance, encouragement and understanding during the exhaustive realization of the project; and for offering this special opportunity to work on a brand new subject.

I am grateful to my colleague Mehmet Yıldız for his contribution, collaboration and help during the company works that the thesis is a part of.

I would like thank the thesis committee members for their advice and comments.

Finally, I would like to thank my family for their endless support and love. I am grateful to my friends for their love, patience and supports during the hard work times.

TABLE OF CONTENTS

ABSTRACT.....	iv
ÖZ.....	v
ACKNOWLEDGMENTS.....	vii
TABLE OF CONTENTS.....	viii
LIST OF FIGURES.....	xii
LIST OF TABLES.....	xv
CHAPTER	
1. INTRODUCTION.....	1
1.1. Introductory Remarks on Hydropower in Turkey.....	1
1.2. Scope and Objective of the Work.....	2
1.3. Literature Survey.....	3
1.3.1. Hydraulic Turbines.....	3
1.3.2. Francis Turbine.....	5
1.3.3. Use of CFD Tools for Hydraulic Turbine Applications.....	8
1.4. Description of the Thesis.....	10
2. DESIGN METHODOLOGY.....	11
2.1. Overview of the Methodology.....	11
2.2. Input parameters.....	13
2.2.1. Discharge.....	13
2.2.2. Head.....	14
2.3. Conventional Design Parameters.....	15
2.3.1. Efficiency.....	15
2.3.2. Power.....	15
2.3.3. Rotational Speed.....	16
2.3.4. Specific Speed.....	18
2.3.5. Reduced Turbine Parameters.....	19

2.3.6. Turbine Type.....	20
2.3.7. Turbine Runner Dimensions.....	21
2.3.8. Shaft Diameter.....	21
2.3.9. Meridional Profile.....	22
2.3.10. Guide Vanes.....	23
2.3.11. Velocity Triangles.....	24
2.3.12. Turbine Working Principle.....	27
2.3.13. Euler Equation.....	30
2.3.14. Blade Angles.....	32
2.3.15. Auxiliary Information for the Determination of Runner Dimensions and Velocity Triangles.....	32
2.4. Implementation of Computer Tools to Turbine Design.....	34
2.4.1. Runner Solid Model Design using Blade Generator.....	34
2.4.2. CFD Application.....	37
2.4.3. Parametrization and Simulation of Stationary Components: Guide Vanes, Stay Vanes, Spiral Case and Draft Tube.....	38
2.4.4. Cavitation.....	40
2.4.5. Verification of Leakage.....	41
3. CFD METHODOLOGY.....	43
3.1. CFD Analysis.....	43
3.1.1. Governing Equations.....	44
3.1.2. Turbulence Models.....	45
3.1.3. Advection Schemes.....	46
3.1.4. Discretization Scheme.....	46
3.1.5. Mesh Connection.....	46
3.1.6. Boundary Conditions.....	47
3.2. Grid Generation.....	48
3.2.1. Topology Definition.....	48
3.2.2. Mesh Generation.....	49
4. APPLICATIONS.....	51
4.1. Project Specifications.....	51
4.1.1. Definition of the Problem.....	51

4.1.2. Input Values.....	51
4.2. Sample Runner Design Procedure.....	52
4.2.1. Turbine power.....	52
4.2.2. Turbine speed.....	53
4.2.3. Specific Speed.....	54
4.2.4. Determination of Preliminary Runner Dimensions.....	54
4.2.5. Determination of the Exit Diameter.....	55
4.2.6. Determination of the Inlet Diameter and Throat Diameter.....	56
4.2.7. Determination of the Wicket Gate Height.....	57
4.2.8. Determination of the Optimum Guide Vane Flow Angle.....	58
4.2.9. Assignment of the Blade Profile.....	60
4.2.10. Determination of the Inlet Velocity Triangles and Blade Angles.....	61
4.2.11. Determination of the Exit Velocity Triangles and Blade Angles.....	62
4.2.12. Blade Shape Transferred to CFD Simulation.....	64
4.3. CFD Simulations.....	66
4.3.1. Summary of the CFD optimization procedure.....	66
4.3.2. Generated Mesh Data for the Final Design.....	68
5. RESULTS.....	69
5.1. Runner Simulations.....	69
5.1.1. Optimization of Meridional Profile.....	72
5.1.2. Leading Edge Shock Free Entrance.....	72
5.1.3. Outlet Swirl.....	75
5.1.4. Prevention of Cavitation.....	75
5.1.5. Mesh Independency.....	76
5.1.6. Effect of Roughness on the Efficiency.....	77
5.1.7. Leakage Simulation and Check.....	78
5.1.8. Final Blade Design.....	78
5.2. Results for the Auxiliary Components.....	82
5.2.1. Spiral Case.....	82
5.2.2. Stay Vanes.....	84
5.2.3. Guide Vanes.....	87
5.2.4. Draft Tube.....	91

5.3. Hydraulic Losses and Summary of Final Results	93
5.4. Discussion of Results.....	93
6. CONCLUSION.....	98
6.1. Summary of the Developed Work.....	98
6.2. Contributions of the Developed Work.....	99
6.3. Future Work.....	99
REFERENCES.....	101
APPENDICES	
A. SAMPLE PICTURES OF TURBINE PARTS.....	107

LIST OF FIGURES

FIGURES

Figure 1. General layout of the turbine in a hydropower project [11].....	3
Figure 2. Turbine and generator [12].....	4
Figure 3. Turbine application chart (Sulzer Hydro) [14].....	6
Figure 4. Flow inside the Francis turbine in the meridional representation.....	7
Figure 5. Francis turbine components [15].....	7
Figure 6. Design methodology chart.....	12
Figure 7. Energy change from headwater to tailwater [25].....	14
Figure 8. Efficiency vs specific speed [28].....	18
Figure 9. Turbine runner types as a function of specific speed [25].....	20
Figure 10. Runner dimensions.....	21
Figure 11. (a) Runner blade meridional profile ; (b) Runner blade isometric view ; (c) Runner blade top view.....	22
Figure 12. Guide vane functioning principle [25].....	23
Figure 13. Inlet and outlet velocities at leading and trailing edges of the runner blade.....	25
Figure 14. Fluid velocity at the runner inlet and outlet.....	26
Figure 15. Flow direction in the meridional representation.....	26
Figure 16. Flow at the guide guide vane exit [26].....	27
Figure 17. Meridional sections of the runner blade.....	34
Figure 18. Blade thickness based on airfoil profile definition	35
Figure 19. Blade profiles after (a) Preliminary design (b) Profile thickness definition (c) Blade angle definition.....	36
Figure 20. Variation of the area graph generated by the blade modeler.....	36
Figure 21. Parametric definition of the draft tube geometry [10].....	40

Figure 22. (a) H-grid type topology (b) J-grid type topology.....	48
Figure 23. Generated mesh layout on the runner blade leading edge.....	50
Figure 24. Hexahedral mesh of the spiral case.....	50
Figure 25. Meridional representation of the runner preliminary dimensions.....	55
Figure 26. Meridional profile definition points.....	57
Figure 27. Guide vane exit flow velocities.....	59
Figure 28. Meridional profile determined by experience and the control points... ..	60
Figure 29. Blade inlet velocity triangles.....	62
Figure 30. Blade outlet velocity triangles.....	63
Figure 31. Change of flow area through the blade passage.....	64
Figure 32. Flow nets generated by the program.....	65
Figure 33. Blade thickness profile for the first test case.....	65
Figure 34. Blade flow passage.....	66
Figure 35. Summary of the CFD optimization procedure.....	67
Figure 36. Runner blade meridional shapes for Case 5 and Case 6.....	72
Figure 37. Case 9 - Pressure on the blade meridional section i3-o3	73
Figure 38. Case 10 - Pressure on the blade meridional section i3-o3	73
Figure 39. Case 9 - Velocity vectors for meridional section i3-o3	74
Figure 40. Case 10 - Velocity vectors for meridional section i3-o3	74
Figure 41. Pressure distribution on blade suction side for Case 12.....	75
Figure 42. Case 12 - Pressure on the blade meridional section with minimum pressure zone.....	76
Figure 43. Runner efficiency and head difference versus number of mesh elements.....	77
Figure 44. Simulated leakage domain plotted with runner blade.....	78
Figure 45. Meridional flow velocity vectors (Case 12).....	79
Figure 46. Variation of total pressure on meridional section (Case 12).....	80
Figure 47. Velocity vectors for meridional section i3-o3 (Case 12).....	80
Figure 48. Velocity vectors for meridional section i4-o4 (Case 12).....	81
Figure 49. Velocity vectors for meridional section i2-o2 (Case 12).....	81
Figure 50. Velocity streamlines (Case 12).....	82
Figure 51. Radial velocity at the spiral case outlet.....	82

Figure 52. Pressure distribution on the spiral case mid-plane.....	83
Figure 53. Velocity vectors on the spiral case mid section.....	83
Figure 54. Blade loading of stay vane.....	84
Figure 55. Distribution of total pressure on stay vane meridional section.....	85
Figure 56. Distribution of pressure in the stay vane passage.....	85
Figure 57. Velocity streamlines in the stay vane passage.....	86
Figure 58. Pressure distribution and velocity vectors on the mid-plane of spiral case and stay vanes.....	87
Figure 59. Blade loading on guide vane.....	88
Figure 60. Distribution of total pressure on guide vane meridional section.....	89
Figure 61. Distribution of pressure in guide vane passage.....	89
Figure 62. Velocity streamlines in guide vane passage.....	90
Figure 63. Simulation of guide vanes with runner blades.....	90
Figure 64. Change of total pressure through the draft tube.....	91
Figure 65. Pressure contours in the draft tube sections.....	92
Figure 66. Velocity vectors on the draft tube mid-section.....	92
Figure 67. Velocity contours and streamlines in the draft tube.....	93
Figure 68. Spiral case solid model modeled after CFD simulations.....	107
Figure 69. Sample drawing for spiral case.....	107
Figure 70. Manufactured spiral case according to final design.....	108
Figure 71. Manufactured turbine runner according to CFD design.....	108
Figure 72. Solid model of the draft tube according to CFD design.....	109
Figure 73. Manufactured draft tube parts according to final design.....	109

LIST OF TABLES

TABLES

Table 1. Main turbine types based on specific speed [13].....	5
Table 2. Generator synchronization speeds [25].....	17
Table 3. Mesh characteristics of each turbine component for final design.....	68
Table 4. Parameters of the selected cases for stage 1.....	70
Table 5. Parameters of the selected cases for stage 2.....	71
Table 6. Summary of hydraulic losses.....	93

CHAPTER 1

INTRODUCTION

1.1. Introductory Remarks on Hydropower in Turkey

As the global tendency for sustainable energy resources has increased, hydropower projects became more important. It is not only sustainable but also a clean energy source if the debate of large dams is not considered as an issue [1].

In Turkey, as in the world, the trade stands for renewable energy. The water power, compared to solar and wind energy, is considered as more valuable and feasible for Turkey; Turkey's topographical variability and suitability of Turkey eases the investment on hydropower projects [2]. This advantage becomes more obvious when the total hydropower potential of Turkey is observed in the global range: Turkey's potential constitutes 1.0% of the world's total hydropower potential [3].

Many hydropower plants have been constructed in Turkey since 1902 starting with small hydropower projects [4]. Turkish engineers have great knowledge about the hydraulic structures like power station buildings, water intake structures, silting basins. Furthermore, in the last two decades, a series of regulations have been enacted to promote renewable energy and hydropower on behalf of Turkish investors [5].

Despite the wide experience and competency in the application of civil works, there still was not any know-how developed in Turkey on the hydropower

equipment design, mainly on turbine design, using state-of-the-art technology such as computational fluid dynamics tools.

1.2. Scope and Objective of the Work

The objective of this thesis is to meet the deficit in the turbine design subject in Turkey. Foreign turbine designers and manufacturers have already implemented the academic research into the application and the industrial work. In the hydraulic turbine area, academic research covers widely the use of CFD tools and their validation. In this purpose, workshops are realized: GAMM workshops are the well known applications [6], [7]. Academic projects are also handled with the collaboration of well known turbine companies and manufacturers like in HYDRODYNA and FLINDT projects [8], [9].

The private sector company Su-Ener was established to develop a national know-how on mechanical design of turbines in Turkey. The methodology covers the steps starting from the preliminary design until the manufacturing stage. The specialty of the work arises from its uniqueness, in Turkey, of developing the design know-how and implementing into it the state-of-the-art technology. This technology includes the use of CFD analysis, parametric modeling and structural analysis tools in the hydraulic turbine design of new projects.

The hydropower project of concern is named Cuniş HPP. It is located near Rize, north of Turkey, in the Black-Sea region. This medium scale project has three identical Francis turbines and the power plant has an installed capacity of approximately 9 MW [10].

The author, being a part of the above project, sets forth the CFD application methodology of the turbine design in this thesis work. The scope of the thesis is the development and improvement of the hydraulic design of a Francis turbine,

especially the Francis runner, using the available state-of-the-art CFD analysis tools.

1.3. Literature Survey

1.3.1. Hydraulic Turbines

Although the thesis work covers the design of a Francis turbine, an introduction to a brief definition of hydropower plant and of hydraulic turbines is warranted. This short information facilitates the understanding of working principles of turbines.

Hydraulic turbines and generators constitute the mechanical equipment of a hydropower plant. As shown in Fig. 1, the water raised upstream of the turbine stores potential energy. Water flows through the penstock, and the potential energy is converted to kinetic energy.

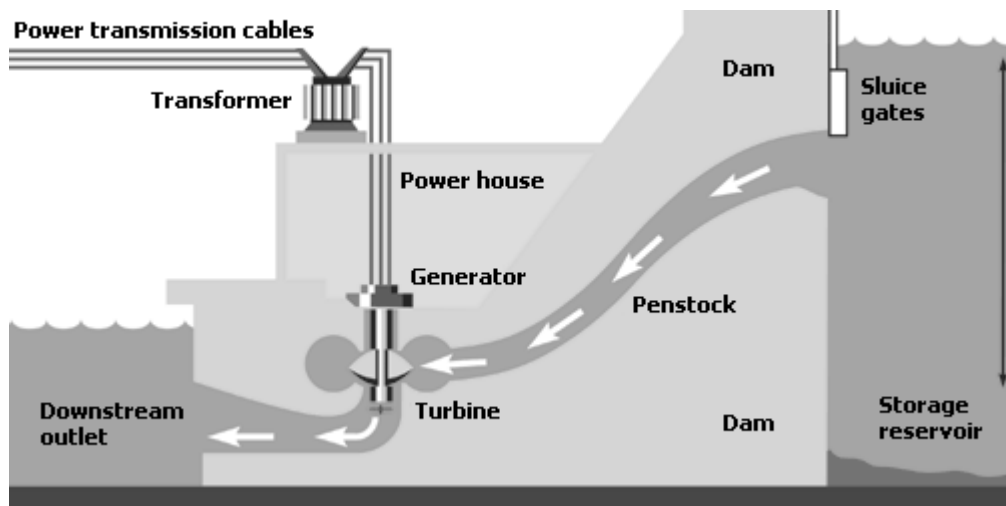


Figure 1. General layout of the turbine in a hydropower project [11]

At the turbine entrance, the pressurized water makes the turbine runner rotate; thus the turbine shaft. Generator shaft is connected to the turbine shaft as shown in Fig. 2 and it produces electrical energy by the rotor-stator action of the generator.

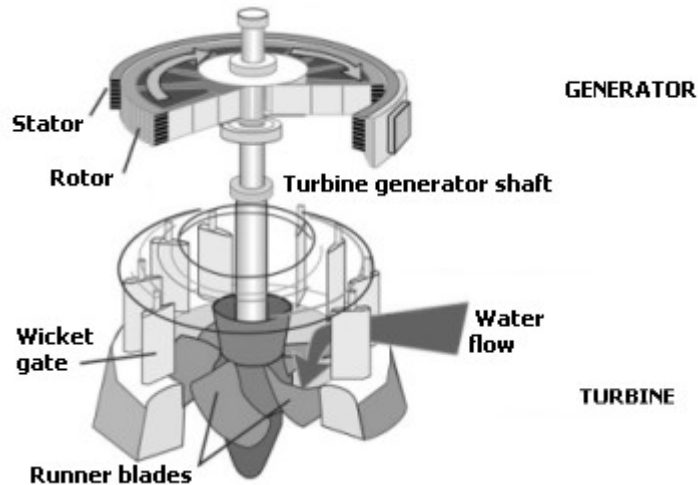


Figure 2. Turbine and generator [12]

Hydraulic turbines are classified in two groups: Impulse type turbines and reaction type turbines.

- *Impulse type turbines:* Working condition is based on the momentum principle. Water hits the runner blades in the form of a water jet. This impact causes a force on the runner blades which, in turn, causes the rotation of the runner. In this type of turbines, the impact of water with the runner blades occur in open air. The flow is therefore not pressurized around the runner. Pelton type represents the best example in this group, widely used for high head applications. [26]
- *Reaction type turbines:* The flow is fully pressurized through the turbine. The potential energy of water is again converted to kinetic energy by a speed rise. In reaction turbine runners; however, the energy is transferred to the runner by an action throughout the blades and not by a local impact. It

uses the action-reaction principle. The water releases its energy continuously, which appears with a pressure decrease along the blades. The most commonly used reaction turbines are Francis and Kaplan types. [26]

Even though there is not a strict rule in practice, a range of application is defined and advised for different turbine types as presented in Table 1. Charts are used by engineers, for the selection of the turbine type, as shown in Fig. 3. Head and discharge are the input parameters defining the turbine speed: they determine the most suitable turbine type.

Table 1. Main turbine types based on specific speed [13]

Turbine type			n_s (rpm)	Maximum H (m)
Impulse	Pelton		7 - 26	1800 - 350
Reaction	Francis	Slow	51 - 107	700 - 410
		Medium	107 - 190	410 - 150
		Fast	190 - 250	150 - 64
	Kaplan		250 - 300	50 - 6

1.3.2. Francis Turbine

Francis turbine belongs to the class of reaction turbines. It is applicable on a wide range of head and discharge values as shown in Table 1. There are several applications of Francis turbines from micro scale producing hundreds of kilowatts to large scales producing hundreds of megawatts of power.

Its large range of applicability makes the Francis turbine profitable. Its applicable range overlays with that of Pelton and Kaplan range as depicted in Fig. 3. In such a case, a Francis turbine may be preferred to a Kaplan due to its compactness; or to a Pelton due to its higher efficiency at the best efficiency point.

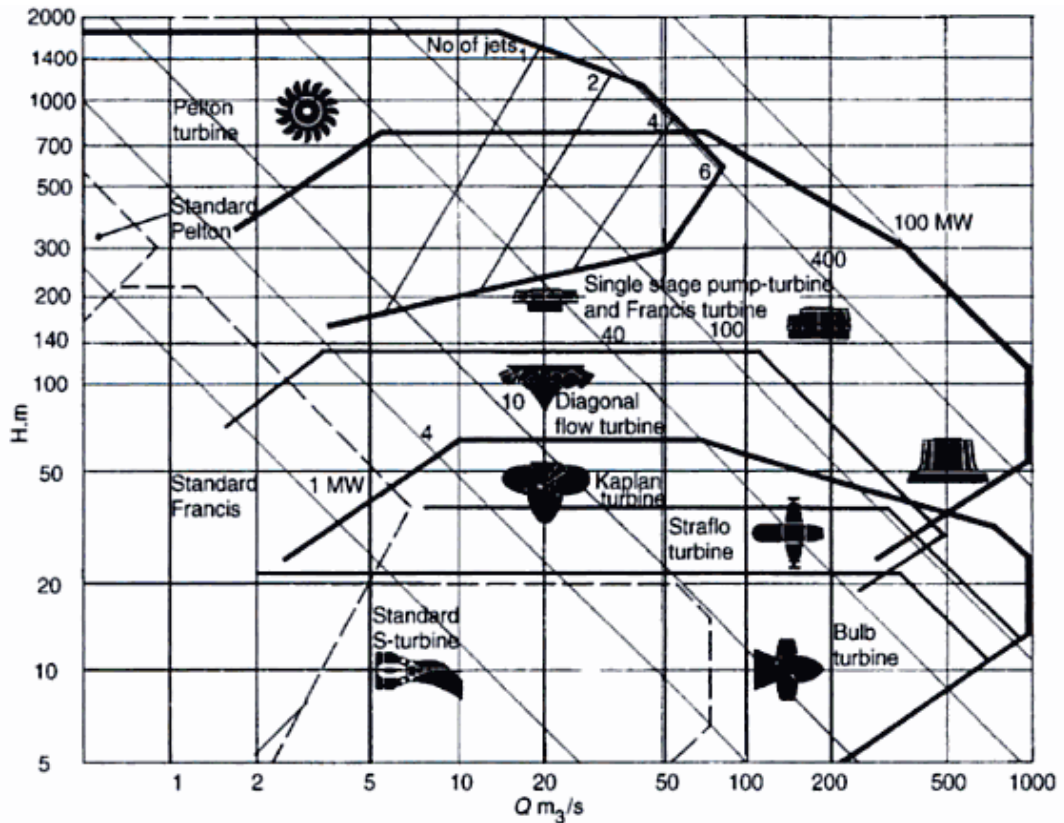


Figure 3. Turbine application chart (Sulzer Hydro) [14]

Another advantage of Francis turbines is their runner: Francis runner blades are always fixed, unlike most of Kaplan runners, which facilitates easier structural design and they are not structurally affected by the fatigue as Pelton buckets. [26]

As shown in Fig. 4, water enters the turbine in a radial direction and leaves it in the axial direction. Hence Francis turbines are also classified as radial-axial turbines due the water inflow and outflow directions.

The flow is pressurized through the Francis turbine. Pressurized water conducted by penstock passes the inlet valve and enters the turbine. The main parts of a Francis turbine are illustrated in Fig. 5. Spiral case distributes the flow radially around the stay vanes in a uniform manner. The flow amount should be more or less uniform in each stay vane passage for a balanced operation.

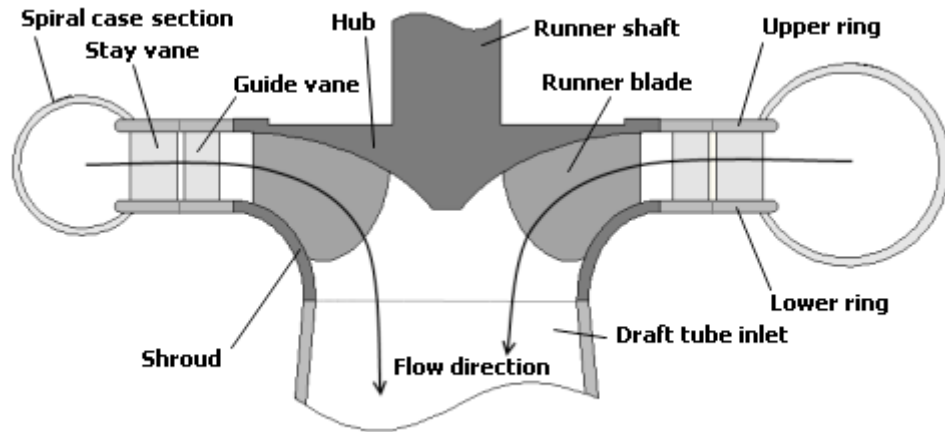


Figure 4. Flow inside the Francis turbine in the meridional representation

The main function of stay vanes is actually structural. They connect the upper and lower ring, to ensure the structural strength [13]. Stay vanes should withstand the tension caused in the spiral case due to the pressurized flow. On the other hand, stay vanes are supposed to provide the correct flow angle and direct the flow through guide vanes with minimum hydraulic losses.

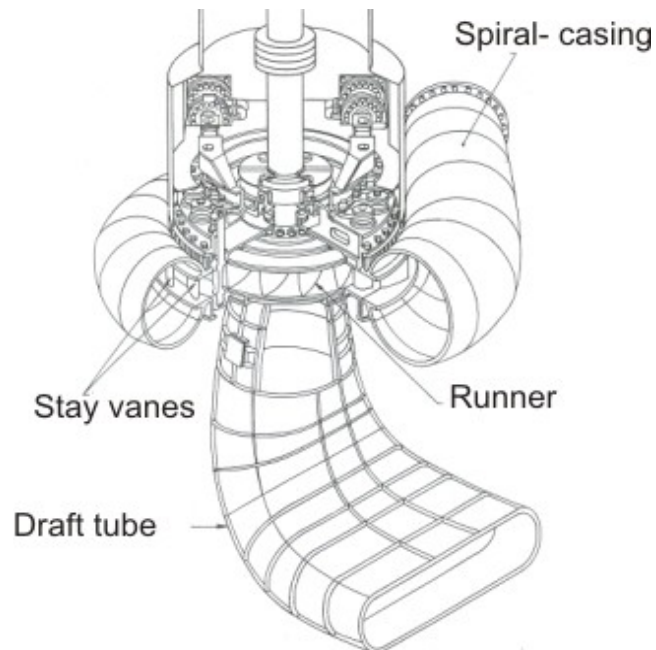


Figure 5. Francis turbine components [15]

Regulation of the flow is managed by the adjustment of guide vanes. They rotate around their axis and alter the net inflow area. This regulation permits correct inflow angle to the runner in varying discharge conditions.

Flow directed by the guide vanes hits the runner blades. Runner blades transform the kinetic energy of the water to rotate the shafts and enable the production of electricity in the generator. Runner is the major component affecting the efficiency thus the generated power.

Once water releases its energy in the runner, it leaves the runner at a minimum pressure. The connection between the runner exit and the tailwater is established by the draft tube. Draft tube increases the water pressure from the runner exit through the tailwater level. Draft tube's cross sectional area increases towards the tailwater so that water is decelerates with minimum hydraulic loss and with maximum pressure recovery. Static pressure is recovered at the tailwater level.

1.3.3. Use of CFD Tools for Hydraulic Turbine Applications

Being in use for over a century, hydraulic turbines are ground on a reliable technology. The growth and competition in the energy market, however, necessitates more production of electricity with less cost, leading to an improvement in the hydropower plant equipment. It is therefore important to increase the efficiency of hydropower plants, namely the efficiency of the turbines.

Turbine efficiency can be increased by an optimization process of the turbine geometry parameters. Successive tests are needed for the improvement of turbine efficiency. Even though it is possible to predict turbine characteristics by model tests in the laboratory; time and budget limitations, prototype restrictions promoted the use of CFD tools for the turbine optimization.

Developing technology enhanced the computational power and led to improvement of turbine design. An accurate prediction of flow inside the hydraulic turbine is nowadays possible by use of state-of-the-art CFD tools [16],[17]. The latest CFD tools are the outcome of several researches handled during the last four decades [18].

CFD knowledge dates back to 1970s [19],[20]; the first applications at the time were limited, for the turbine analysis, to potential flow solutions mainly in two dimensions [18]. Majority of turbine runners have, nevertheless, complex geometries which can not be solved in 2D. Need for more complex discretization schemes, necessity for vorticity and viscosity terms led to the development of 3D codes involving Euler equations followed by codes involving Reynolds-Averaged Navier-Stokes, RANS, equations.

CFD codes solving either Euler or RANS formulations evolved over time and yielded good results [18]. It is possible to determine the turbine performance using CFD tools. The turbine performance is usually presented by a plot showing the turbine efficiency under varying head and discharge values. This plot is named efficiency hill chart of the turbine. A numerical hill chart can be created from CFD simulations [16]. Experiments are conducted and the results are compared with CFD results. A good match is usually obtained between the test results and CFD results [21], [22]. CFD tools in question include 3D Euler and 3D Navier-Stokes codes; either developed by institutions or commercially available ones.

The high accuracy level in the CFD results promoted the use of CFD tools in rehabilitation projects [23],[24]. Even in some projects, CFD simulations are presumed to be accurate enough and model tests are not performed [24].

Validation of the lately developed tools prove that the accuracy of CFD tools are very high. This made the power of CFD tools undeniable in the design process.

1.4. Description of the Thesis

The main hydraulic theory and CFD application on Francis turbine design is explained throughout the thesis.

The thesis work consists of five chapters. In Chapter 1, some definitions and preliminary information are given about the hydraulic turbines, particularly about the Francis turbines. The definition of hydraulic turbines is followed by a short literature review: A short information on CFD history on hydraulic turbomachinery is given and previous CFD applications for hydraulic turbines are presented.

The basics of the turbine hydraulics are explained throughout methodology section in Chapter 2. Methodology chapter covers the steps of the turbine design, including the conventional design and the implementation of computer tools. Working principles of turbines and the theory of turbomachinery is investigated in detail for a good understanding of the design parameters.

In Chapter 3, design of an actual turbine is explained: turbine properties, based on the generated methodology steps, are enumerated. In Chapter 4 the CFD methodology is described.

In Chapter 5 CFD results are evaluated where several applications are demonstrated. As the main design work focuses on the turbine runner, the theoretical design computation of the runner is given in detail. The details of computations for auxiliary components are not given. Instead, the necessary targeted values are explained. Finally, a short summary of the developed work is given in Chapter 6.

CHAPTER 2

DESIGN METHODOLOGY

2.1. Overview of the Methodology

Hydropower projects are developed based on the allocation of the project resources and requirements. Available resources like flow duration data, geological conditions determine the design parameters. Two design parameters, operational head range and discharge variation, are designated by the final design of hydraulic structures. Turbine design and selection is then possible based on the design operation condition. The design operation condition implies the design head, H_d , and the design discharge, Q_d available for each turbine.

Each hydropower project necessitates a different turbine design. A methodology is developed, as shown in Fig. 6, to obtain a Francis turbine design specific to a project. Prior to the development of the methodology, a survey is conducted on theoretical and technical capabilities. Technical capabilities involve the modeling tools and available CFD codes. A literature survey is handled both on hydraulic machinery theory and on the applications of CFD tools. Validation, interpretation and applications of CFD tools are investigated.

The first step of the methodology is the preliminary design of the turbine. The preliminary dimensioning is based on the net head value available at the turbine inlet and the discharge in the system. Matlab codes are used for the determination of the initial dimensions and the turbine parameters: They include some empirical

and theoretical formulas. The codes are generated in Matlab. The theory and the procedure followed in their formation, and the necessary information for CFD analysis and design, are presented in detail in the following chapters.

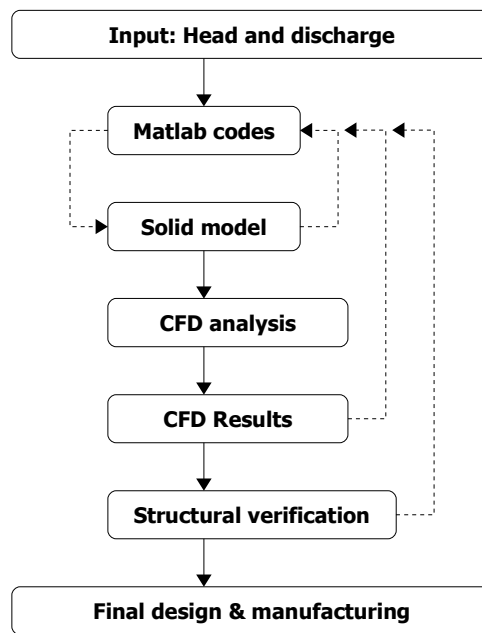


Figure 6. Design methodology chart

Preliminary design relies on experimental techniques, conventional design procedures and on hydraulic machinery theory. Preliminary solid model dimensions are subject to CFD analysis for the evaluation of the hydraulic performance. CFD analyses enable the determination of undesirable flow conditions such as flow separation, cavitation zones which are not possible to predict in the conventional design techniques.

A design loop exists between solid model design parameters and CFD simulation results. Preliminary design is enhanced by the interaction of successive CFD results with design parameters of the turbine. This is an iterative process leading to an optimum working condition of the turbine, especially of the turbine runner. It is

worth mentioning that the maximum turbine efficiency is not reached at the design operation condition but at a part load operation. The turbine efficiency is slightly lower than the maximum efficiency under the design head and design discharge: this case is named as the turbine optimum working condition throughout the work. It is worth noting that approximately 96% of hydraulic losses occur in the runner in a Francis turbine. Therefore, the main design work therefore focuses on the runner blades.

Slight changes in the solid model of the turbine, especially in the runner, leads to an optimized geometry of the turbine with optimized efficiency and flow dynamics. The problematic areas are subject to change in order to reach the targeted efficiency under design head and design discharge. An optimized turbine geometry is checked for structural safety and is ready for manufacturing. Structural safety checks are not discussed in this thesis as they are out of the scope of this work.

2.2. Input parameters

Main input parameters are the operational design discharge and head values of the hydropower plant.

2.2.1. Discharge

Hydraulic structures are designed according to a specific design discharge. During the feasibility analysis of a hydropower project, various design discharge alternatives are evaluated for optimum energy production. Once the optimum design discharge is selected, the hydraulic structure, the number of the water ways and the number of turbines are decided and the turbine design discharge, Q_d , is determined.

2.2.2. Head

Discharge sets the hydraulic losses in the system. Net head of the system is determined and thus a design head value. As the type of project, i.e. whether it has a storage or it is run-of-river type, indicates the operating head range. The turbine properties should conform the project properties. Once the design head and discharge values are determined, hydraulic turbine equipment can be designed accordingly.

Design net head of the turbine (named also as the “head of the turbine”) is the energy difference between the inlet and outlet of the turbine, as shown in Fig. 7. It can be defined by equation (1).

$$H_d = H_s - h_L \quad (1)$$

where H_s is the gross static head available for the turbine, i.e. difference between the head water elevation and tail water elevation; h_L is the head loss term including hydraulic losses in the water conduits from head water to the turbine and from the turbine exit to the tail water [26]. Losses inside the turbine are implied by the turbine efficiency term η .

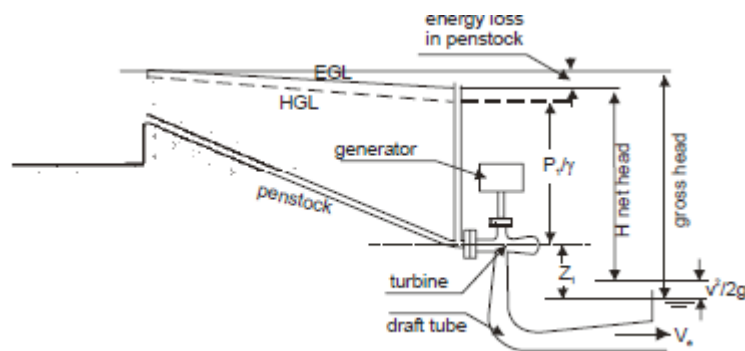


Figure 7. Energy change from headwater to tailwater [25]

2.3. Conventional Design Parameters

The conventional design parameters, introduced below, combined with hydraulic turbomachinery theory, permits the computation of the turbine capacity and the preliminary design of the entire turbine geometry. The conventional design parameters of the turbine include mainly efficiency, power, rotational speed, specific speed, runner blade angles.

2.3.1. Efficiency

Potential energy of the water is converted to kinetic energy by the rotation of the turbine runner. This energy is transmitted by the shaft to the generator where it is transformed to electrical energy. Ability of the hydraulic turbine to transmit this potential by rotation is named as the efficiency of the turbine.

Different efficiency classifications exist such as the volumetric efficiency, hydraulic efficiency and overall efficiency of the turbine [27]. It should be noted that throughout this work, the turbine hydraulic efficiency – the ratio of the turbine shaft power to the available hydrostatic power- is used and investigated as the turbine efficiency η . Losses due to friction of mechanical parts are not considered. Turbine efficiency, η , includes the turbine leakage losses computed and turbine hydraulic losses analyzed in CFD.

2.3.2. Power

The available net head for the turbine is determined after the losses in the waterways, such as penstock losses, are excluded in equation (1). The total hydraulic power, P , available for the turbine is then calculated from the net head H_d of the turbine.

$$P = \rho g Q_d H_d \quad (2)$$

where g is the gravitational acceleration in m/s^2 ; Q_d is the design discharge available for one turbine in m^3/s ; H_d is the design head of the turbine in m .

The power generated by the hydraulic turbine is calculated by the following equation:

$$P_d = \rho g Q_d H_d \eta \quad (3)$$

where P_d is the power generated by the hydraulic turbine in *Watts*.

In order to express the power in “metric horsepower”, the following transformation equations can be used:

$$P_{hp} = \frac{P_d}{0.7355} \quad \text{or} \quad P_{hp} = 1.36 P_d \quad (4)$$

2.3.3. Rotational Speed

In the preliminary stage, the rotational speed n of the runner can be calculated based on design head and power to be generated at the design head value :

$$n = n_q \frac{H_d^{1.25}}{P_d^{0.5}} \quad (5)$$

$$n_q = \frac{C_{nq}}{H_d^{0.535}} \quad (6)$$

$$c_{nq} = \min(2600; 2600 - (200000 - P_d)/365) \quad (7)$$

where n is in *rpm* ; n_q is the specific speed of the runner in terms of *metric hp* ; P_d is the turbine power in *kW* .

If the runner rotational speed and the generator rotational speed are the same, the runner of the turbine may be directly connected to the generator by the same shaft. If the generator rotational speed is different from the runner, turbine shaft is coupled to generator shaft by a transmission. In either case the standard generator should reach a synchronous speed depending on the number of poles and on the frequency as listed in Table 2.

Table 2. Generator synchronization speeds [25]

Number of poles	Frequency		Number of poles	Frequency	
	50 Hz	60 Hz		50 Hz	60 Hz
2	3000	3600	16	375	450
4	1500	1800	18	333	400
6	1000	1200	20	300	360
8	750	900	22	272	327
10	600	720	24	250	300
12	500	600	26	231	377
14	428	540	28	214	257

The calculated rotational speed n in equation (5) is not the actual rotational speed of the runner. This rotational speed n and the design head H_d determine together the number of poles necessary in the generator. Thus only certain rotational speeds are allowed for the runner because of the pole number restriction. These distinct rotational speeds are called synchronous speeds and can be calculated by the following formula:

$$n_{sync} = \frac{120 f}{2(\text{number of poles})} \quad (8)$$

where n_{sync} is the synchronous rotational speed of the runner in *rpm* ; f is the frequency in *Hertz* , equal to 50 or 60 *Hertz* depending on the regional grid.

It is clear that head and discharge values determine not only the power but also the speed of rotation of the turbine and the specific speed. Specific speed is the main parameter in turbine modeling; it affects the efficiency of the turbine (Fig. 8) and determines the type (Fig. 9).

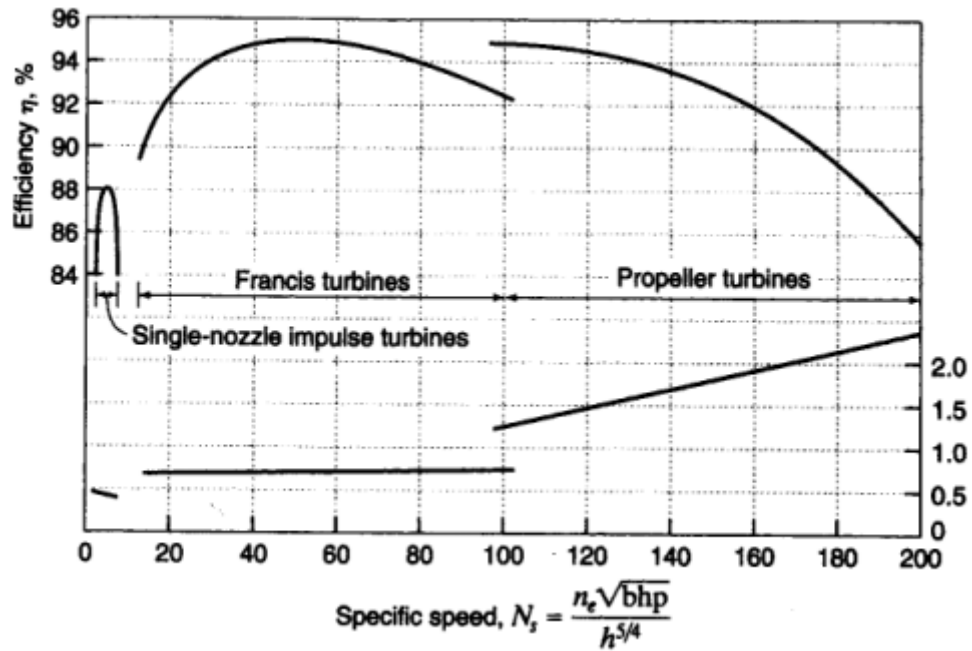


Figure 8. Efficiency vs specific speed [28]

2.3.4. Specific Speed

Specific speed, n_s , of a turbine is by definition “the runner speed necessary to generate 1 unit of power (here in *hp*) under a head of 1 meter”.

$$n_s = n_{sync} \frac{P_d^{0.5}}{H_d^{1.25}} \quad (9)$$

where n_{sync} is the synchronous rotational speed of the turbine runner in *rpm* ; P_d is the turbine power in *metric hp* ; H_d is the design head in *m* ; n_s is the specific speed calculated using *metric hp* units.

Other proposed specific speed formulation is given in the following equation

$$n_q = n \frac{\sqrt{Q_d}}{H_d^{3/4}} \quad (10)$$

where Q_d is in m^3/s ; and H_d is in *m* .

2.3.5. Reduced Turbine Parameters

Dimensionless parameters can be used to define turbine characteristics. Two important parameters are the discharge and energy coefficient. Discharge coefficient, φ , is calculated by [31]:

$$\varphi = \frac{Q}{(\pi \omega R_{ref}^3)} \quad (11)$$

where Q is the discharge in m^3/s , ω is the rotational speed of the turbine in $1/s$, and R_{ref} is the reference radius of the runner in *m* . Energy (or head) coefficient is calculated by [31]:

$$\psi = \frac{2g H_d}{\omega^2 R_{ref}^2} \quad (12)$$

The flow and head coefficients of the turbine are used to check the turbine efficiency and cavitation performance.

2.3.6. Turbine Type

Head and discharge values are the primary indicators of turbine selection, as demonstrated in Fig. 3. It is also shown in Table 1 that the specific speed range is another indication of the turbine type.

Francis turbine runners are classified as slow, medium or high speed depending on their specific speed. This classification implies different runner shapes. Representative runner meridional profiles for different specific speeds are illustrated in Fig. 9. These profiles do not restrict the design; they provide an overall idea over the runner geometry of the turbine to be designed.

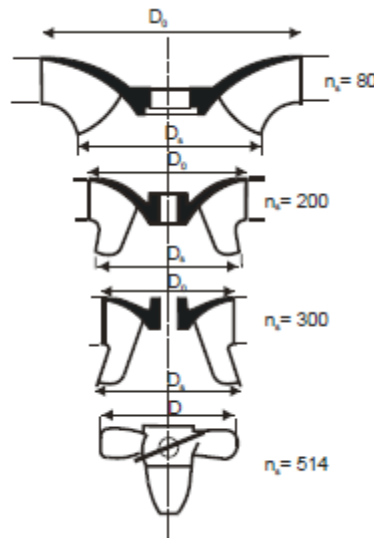


Figure 9. Turbine runner types as a function of specific speed [25]

2.3.7. Turbine Runner Dimensions

After determining the turbine synchronous speed, the overall geometry of the Francis turbine runner is determined based on empirical curves built in the Matlab codes. Therefore once the runner speed, specific speed and the design head are known, runner inlet and runner exit diameters and the wicket gate height are determined from the empirical curves. Preliminary blade model can be formed.

A model of the preliminary blade model is generated according to: Turbine entrance diameter D_1 , throat diameter D_2' , exit diameter D_2 , maximum outside diameter D_{max} , wicket gate height b_0 , wicket gate diameter D_g and shaft diameter D_s as illustrated in Fig. 10.

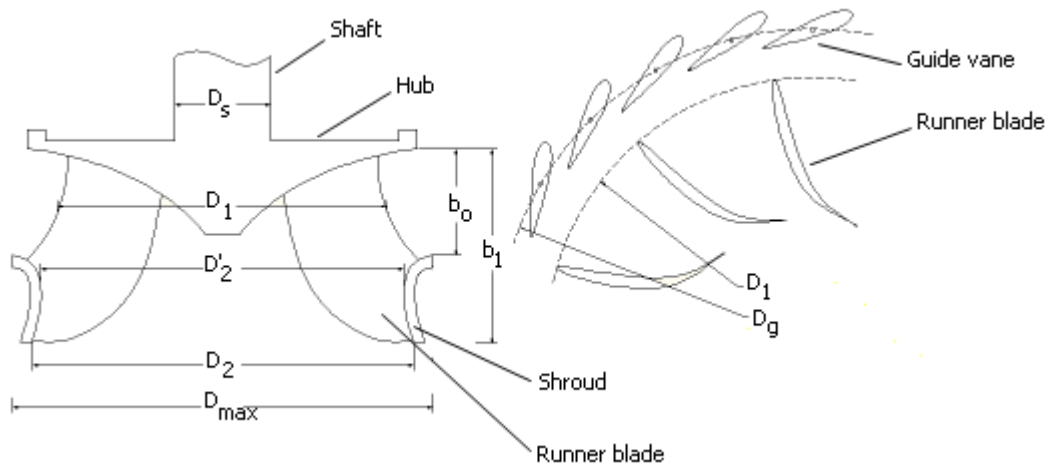


Figure 10. Runner dimensions

2.3.8. Shaft Diameter

Shaft diameter is calculated from the empirical equation:

$$D_{shaft} = 105 \left(\frac{P_d}{n} \right)^{0.35} \quad (13)$$

Shaft diameter is important in the determination of the preliminary runner geometry. Runner dimensions should allow enough space for a structurally safe shaft; runner blades should be designed accordingly.

2.3.9. Meridional Profile

The preliminary geometry definition of the turbine runner is performed using the meridional profile representation. Meridional profile is a surface of revolution, a projection of the blade profile on a radial section, where blade cross section layers are defined.

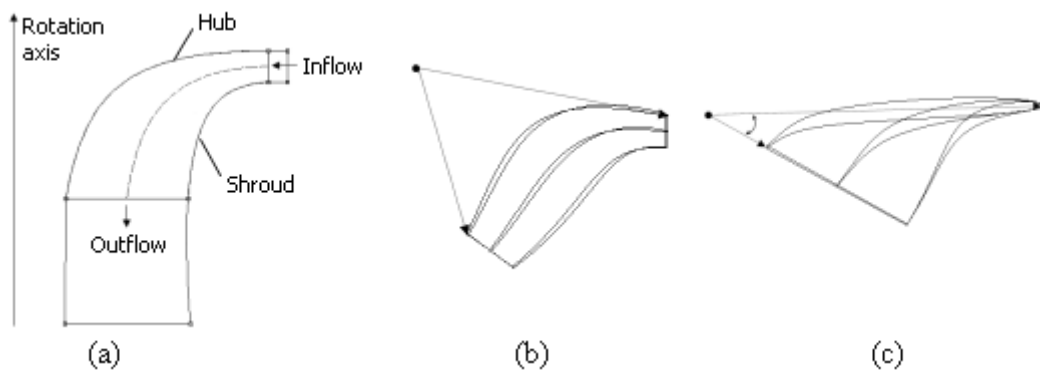


Figure 11. (a) Runner blade meridional profile ;
(b) Runner blade isometric view ; (c) Runner blade top view

As shown in Fig. 11 (a), midsection line in the meridional profile represents the mid cross-section of the 3D blade in Fig. 11(b). The meridional profile definition is useful for the inlet and outlet representation, hub and shroud profile determination and blade angle definitions.

2.3.10. Guide Vanes

Guide vanes distribute the flow around the runner; they rotate about their axis for the flow adjustment as illustrated in Fig. 12. Their rotation center should be located in order not to disturb the runner blades in the maximum opening case.

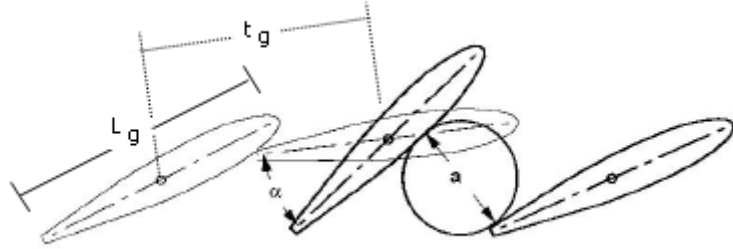


Figure 12. Guide vane functioning principle [25]

The diameter of the circle passing from the guide vane center, D_g as shown in Fig. 10, is generally chosen as 1.16 of the runner inlet diameter [26]. Once D_g is known and number of guide vanes is determined, generally taken as 12, 16 or 24 in the design. Therefore it is possible to calculate a guide vane length so that in the closed position they will overlap and not permit water passage. As a rule of thumb equation (14) is applied for guide vane length choice [26].

$$L_g/t_g = 1.1 \quad (14)$$

In equation (14), L_g represents guide vane camber length and t_g represents the vertical distance between guide vanes. A complete closure of guide vanes is necessary, guide vane length is therefore always slightly larger than the pitch distance.

Guide vane length with 10% overlap at closed position is obtained using

$$L_g = \frac{\pi D_g}{\text{number of guide vanes}} \frac{1}{0.9} \quad (15)$$

Distance between successive guide vanes are computed as follows assuming the arc length is nearly equal to the linear distance between guide vane center of rotations:

$$t_g \approx \frac{D_g \pi}{\text{number of guide vanes}} \quad (16)$$

2.3.11. Velocity Triangles

Flow velocity \mathbf{v} represents the fluid velocity in stationary frame and \mathbf{u} is the blade circumferential velocity due to rotation such as

$$\mathbf{u} = \omega r \quad (17)$$

where ω is the angular rotational speed of the runner in s^{-1} and r is the radial distance from the rotation center of the runner.

By extracting the blade circumferential velocity vector \mathbf{u} from the fluid velocity vector \mathbf{v} , the relative fluid velocity can be obtained with respect to the runner. The fluid velocity vector \mathbf{w} in the rotational frame of reference is therefore obtained. (Fig. 13).

In the notation, the subscript “1” represents the runner inlet and the subscript “2” represents the runner outlet. Subscript “0” is used for guide vane velocities and outlet diameter. Blade leading edge and trailing edge angles are defined, in Fig. 13, as δ_1 and δ_2 respectively.

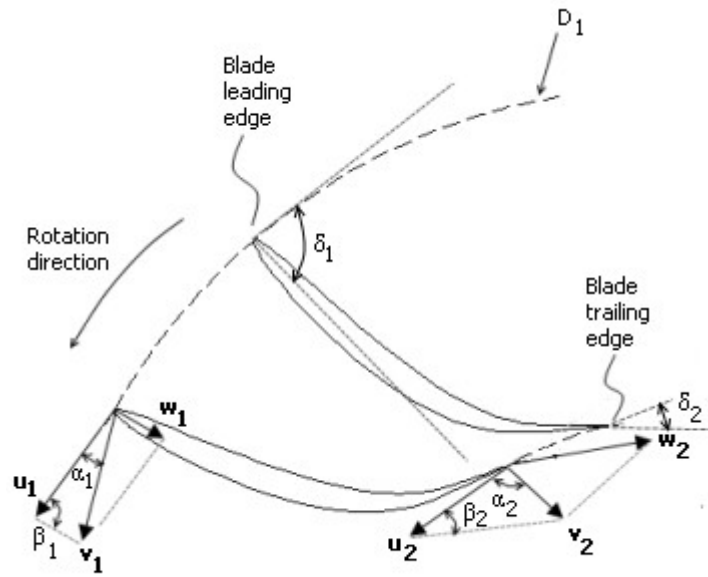


Figure 13. Inlet and outlet velocities at leading and trailing edges of the runner blade

Fluid velocity vectors are defined by a radial vector component, v_r , and a circumferential vector component, v_u (Fig. 14):

$$\mathbf{v} = \mathbf{v}_r + \mathbf{v}_u \quad (18)$$

The flow enters the turbine radially and leaves the runner in an axial direction as shown in Fig. 15. The meridional velocity components coincide with the radial components in the radial flow direction, i.e. at the guide vanes and runner inlet level: $v_{0r} = v_{0m}$ and $v_{1r} = v_{1m}$ respectively.

As the flow leaves the runner in the axial direction, the radial term at the runner outlet is therefore meaningless: The meridional component v_{2m} is used in the following computations.

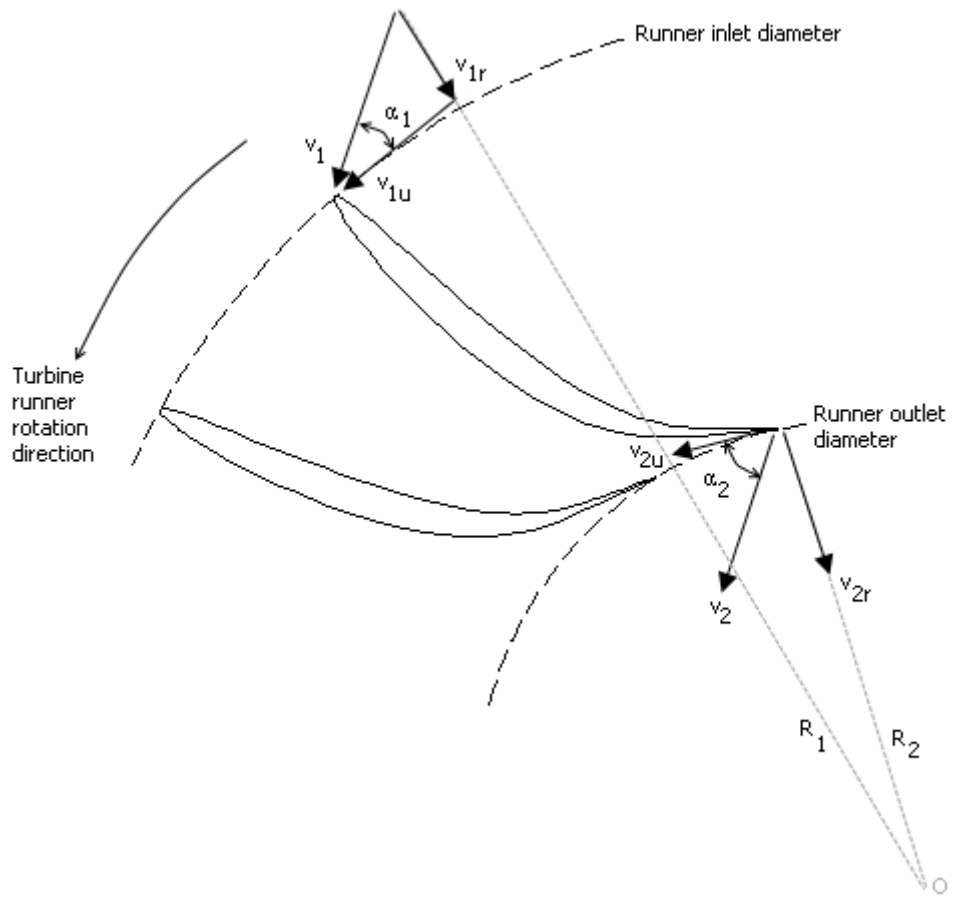


Figure 14. Fluid velocity at the runner inlet and outlet

The flow leaving the guide vanes is represented by the velocity vector, v_0 . (Fig. 16) If cylindrical coordinates are used for the design, this velocity vector can be expressed in terms of circumferential and tangential components:

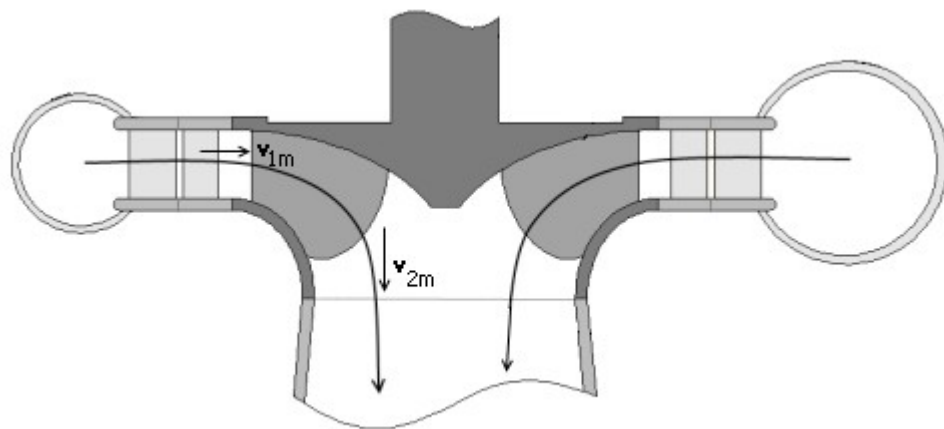


Figure 15. Flow direction in the meridional representation

The dot product in equation (20) can be written in the form of

$$\Gamma = \oint_C \mathbf{V} \cos(\alpha) d\mathbf{l} \quad (21)$$

where α is the angle between the velocity vector \mathbf{V} and the differential line vector $d\mathbf{l}$.

By using the circulation definition of equation (21), the circulation at the guide vane exit diameter can be expressed by

$$\Gamma_0 = (\pi D_0) v_0 \cos(\alpha_0) \quad (22)$$

where Γ_0 is the circulation created by guide vanes; D_0 is the guide vane exit diameter at optimum guide vane opening; v_0 is the average flow velocity at the guide vane exit and α_0 is flow angle with the tangential direction, if an averaged flow is considered at the guide vane exit [26].

After determining the circulation value at guide vane exit, it is important to investigate the circulation at the runner inlet. A short demonstration is needed for this purpose.

A fluid particle of mass m is considered in the gap area between the guide vane exit and the runner inlet, at a distance r from the center of rotation 0, as shown in Fig. 16. Angular momentum is defined by

$$L = m v_u r \quad (23)$$

where L is the angular momentum; v_u is the circumferential (tangential) velocity to the rotation. Torque (moment) around the machine rotation center 0, is obtained by

$$M_0 = \frac{dL}{dt} \quad (24)$$

where M_0 is the moment around 0 created by the surface forces of mass m .

Equations (23) and (24) lead to

$$M_0 = \frac{d(m v_u r)_0}{dt} \quad (25)$$

The forces acting on the particle of mass m is illustrated in Fig. 16. The pressure forces on the particle does not create a moment about rotation axis 0; and very small shear forces around the mass particle are neglected [26]. It is therefore concluded that the moment created by the forces of mass m is zero

$$M_0 = 0 \quad (26)$$

and the value of angular momentum is constant

$$m v_u r = \text{constant} \quad (27)$$

As the water particle mass is constant, equation (28) is obtained which is named as the “law of conservation of velocity momentum.”

$$v_u r = \text{constant} \quad (28)$$

In order to determine the runner inlet circulation from the momentum conservation, equation (22) is transformed in the from of equation (29):

$$\Gamma_0 = 2 \pi R_0 v_{0u} \quad (29)$$

From the definition of circulation, the circulation value at runner inlet is

$$\Gamma_1 = 2\pi R_1 v_{1u} \quad (30)$$

where Γ_1 is the circulation at the runner inlet, R_1 is the radius at the runner inlet.

Knowing that the $v_u r$ is constant throughout the radial line, following equality can be obtained

$$R_0 v_{0u} = R_1 v_{1u} \quad (31)$$

and it can be deduced that

$$\Gamma_1 = \Gamma_0 \quad (32)$$

In conclusion, even a gap space exists between the guide vane exit and the runner inlet, it can be presumed that the circulation of the free fluid flow remains unchanged from the guide vane exit to runner inlet.

2.3.13. Euler Equation

Equation (25) can be applied to a control volume enclosing the turbine runner. Runner inlet is assumed as the inflow control surface and the runner outlet is the outflow control surface. There is no inflow or outflow on other surfaces. In this case the time rate of change of angular momentum is equated to the net momentum flux through the control surfaces as

$$M_0 = \frac{d(m v_u r)_0}{dt} = m \frac{d(v_u r)}{dt} = \rho Q (v_{2u} R_2 - v_{1u} R_1) \quad (33)$$

if average values are used [26]. Remembering the definition of power in terms of momentum:

$$P_d = M_0 \omega \quad (34)$$

and combining the equations (33) and (34) with the definition of turbine power leads to the following equation:

$$\rho g Q_d H_d \eta = \rho Q (v_{2u} R_2 \omega - v_{1u} R_1 \omega) \quad (35)$$

Substituting the circulation terms at the runner inlet and outlet

$$\Gamma_1 = 2 \pi R_1 v_{1u} \quad (36)$$

$$\Gamma_2 = 2 \pi R_2 v_{2u} \quad (37)$$

respectively and the relations

$$R_1 \omega = u_1 \quad (38)$$

$$R_2 \omega = u_2 \quad (39)$$

into equation (35), one obtains

$$H_d \eta = \frac{1}{g} (u_1 v_1 \cos \alpha_1 - u_2 v_2 \cos \alpha_2) = \frac{\omega}{g 2 \pi} (\Gamma_1 - \Gamma_2) \quad (40)$$

The above equation, equation (40), is the main energy equation for turbines and named as the “*Euler equation*”.

Another form of the Euler equation can be derived from Bernoulli equation and specific energy. It is in terms of velocities and useful to directly relate turbine inlet and outlet velocities to the head and efficiency [26]:

$$H \eta = \frac{v_1^2 - v_2^2}{2g} + \frac{u_1^2 - u_2^2}{2g} + \frac{w_2^2 - w_1^2}{2g} \quad (41)$$

2.3.14. Blade Angles

The angle β is the angle formed between the circumferential blade velocity and the fluid velocity in the rotational frame of reference, as depicted in Fig. 13.

At the best operation condition, blade angles, δ , are expected to coincide with the flow angles in the rotational frame, β . A shift between the directions of velocity vector w and the blade angle δ would cause a flow separation or shock loss at the LE (leading edge) [26]. Any flow separation or shocking entrance decreases the turbine efficiency.

Construction of velocity triangles are of major importance in the blade angle definition. Blade angles constitute the most important parameters in the solid model formation and in the optimization of CFD analyses.

2.3.15. Auxiliary Information for the Determination of Runner Dimensions and Velocity Triangles

The preliminary runner dimensions described in section 2.3.7. relies on empirical data. The preliminary dimensions must be checked against and compared with some other theoretical and/or empirical information in order to construct the velocity triangles. These include:

- Meridional flow velocity at the runner exit: for the determination of the meridional velocity at the runner exit the following formula after Petermann [29] is used.

$$v_{2m} = \sqrt{2 g H_d \varepsilon} \quad (42)$$

where δ_r , k , β_{oa} , ε are design variables which are function of turbine type and specific speed.

- The average radial velocity at the runner inlet: Inlet velocity is related to the runner outlet velocity v_2 by the following equation:

$$v_{1r}/v_{2m} = a \quad (43)$$

where a is a ratio coefficient depending on turbine specific speed [29].

- Circumferential velocity at the blade leading edge. It is obtained using the following formula:

$$u_1 = \frac{v_{1m}}{2 \tan \beta} + \sqrt{\left(\frac{v_{1m}}{2 \tan \beta}\right)^2 + g H_d \eta} \quad (44)$$

where β is selected according to the turbine classification [29].

Detailed use of the above formulae, with the Blade generator and CFD tools, is presented in the application chapter.

2.4. Implementation of Computer Tools to Turbine Design

2.4.1. Runner Solid Model Design using Blade Generator

Since the boundaries of the flow passage should be defined prior to the mesh generation, a solid model of the runner should be created before CFD analysis. Runner blades are created using the *BladeGen* tool of ANSYS v.11. *BladeGen* is selected for the design because it is known to provide rapid simulations and optimization when coupled with the CFX fluid analysis tool of ANSYS [30]. As the blade modeler is coupled to the CFD code, individual parameters can be modified rapidly and transferred again to CFD solver for performance evaluation.

The blade definition is performed on meridional representation. Several meridional sections are defined, as illustrated in Fig. 17. Section 1 represents the shroud section of the blade and section 5 represents the hub section. Any design formulation does not exist for hub and shroud profile curves: they are adjusted manually based on literature survey and on experience gained during the applications. The adjustment can be accomplished using Bézier or spline control points.

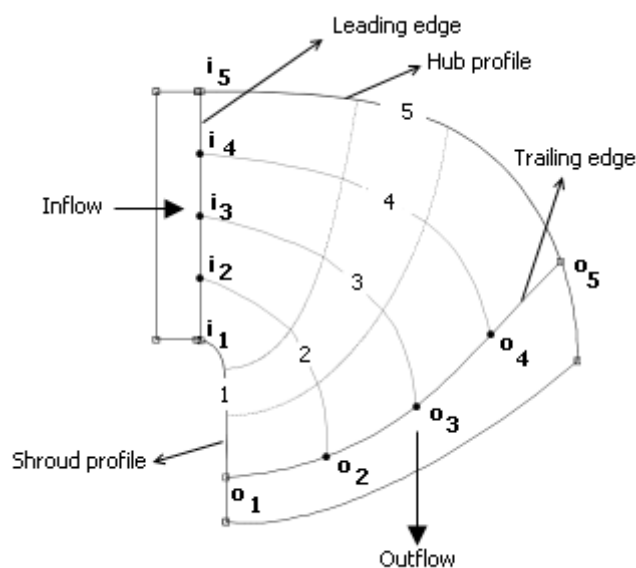


Figure 17. Meridional sections of the runner blade

The blade parameters are defined for each meridional section. These parameters include the number of blades, blade thickness profile and blade angles.

- Number of blades are determined based on literature survey and experience gained during the application process.
- Blade thickness profile is also determined based on knowledge, experience and trial-and-error in the CFD simulations. Generally an airfoil profile is assigned to each section, as shown in Fig. 18.

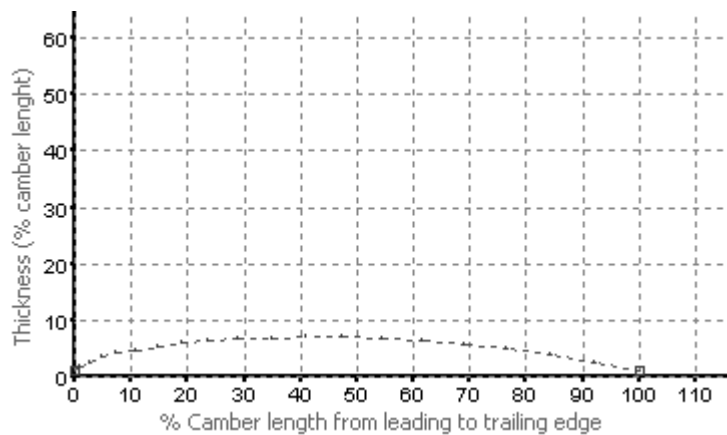


Figure 18. Blade thickness based on airfoil profile definition

- Blade angles δ are deduced from the theoretical calculation of the velocity triangles and CFD optimization process. Shape of the runner blade after the blade angle assignment is illustrated in Fig. 19.

As it was shown in Fig. 6, there is an interaction between the Matlab codes and the solid model. Here Matlab codes include the theoretical design formulations given in the previous sections. Solid model is the runner blade model in 3D.

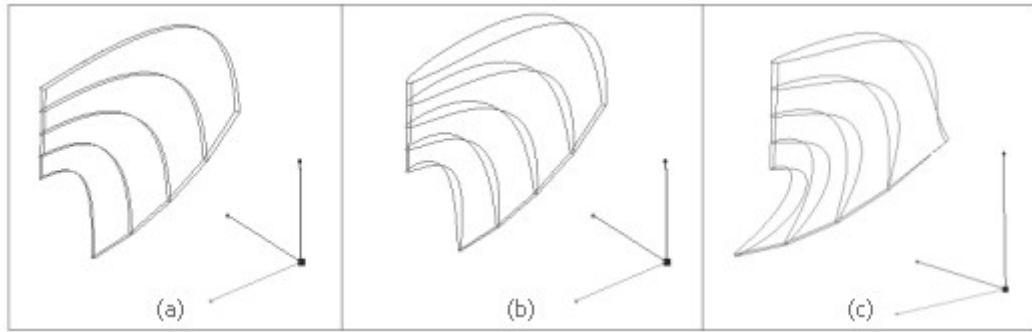


Figure 19. Blade profiles after (a) Preliminary design (b) Profile thickness definition (c) Blade angle definition

In the conventional design computations, runner inlet and outlet areas are approximated. The cross sectional area at the blade leading edge is curved; direct calculation of the exact area is not possible. However the blade generator provides the flow area between the blades throughout the flow passage, as shown in Fig. 20. In order to have more accurate results during the runner blade optimization, corrected inflow and outflow areas are used.

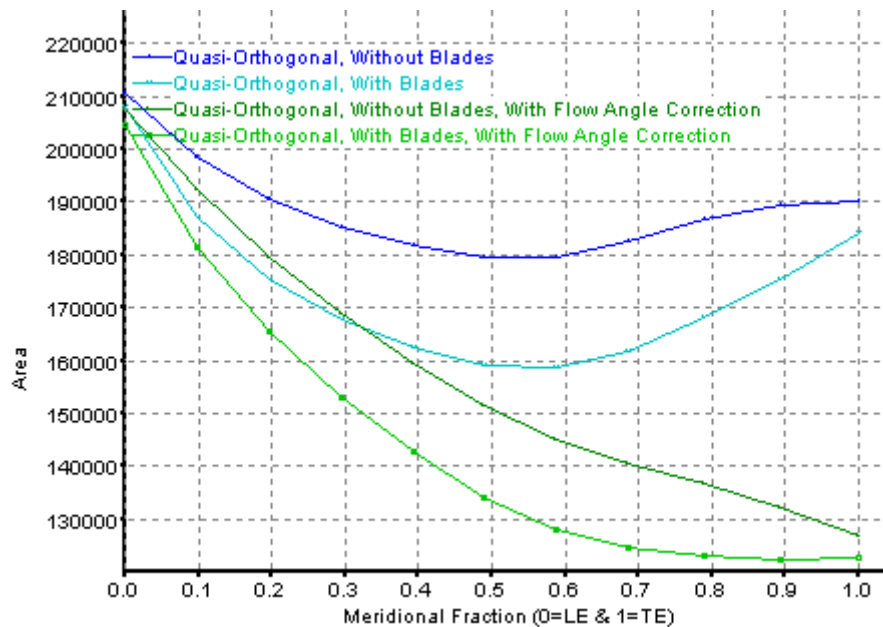


Figure 20. Variation of the area graph generated by the blade modeler

As shown in Fig. 17, leading and trailing edges are defined by five points. In the conventional design method, the coordinates of points are investigated manually, including some error. But the computation of velocity triangles vary at each point because the rotational velocity is different at different radial locations. Blade generator eases this computation of velocity triangles by directly providing the point coordinates of meridional sections. Point coordinate outputs are used as input for the velocity triangle computation in Matlab codes. Matlab codes provide the blade angles specific to each point as output, based on theoretical formulas given in the previous sections.

2.4.2. CFD Application

The theoretical design of the turbine components does not always provide the estimated turbine performance. Unexpected flow behaviour may result due to the assumptions in the theory or interactions of components.

In this methodology the designed turbine is analyzed using computational fluid dynamics (CFD). Adequate design parameters include the spiral case outlet flow distribution, runner blade pressure distribution, draft tube pressure recovery, etc. Geometrical parameters are optimized by modifying the turbine geometry according to CFD results. Undesired peak pressures, flow separations are detected by CFD simulations. The parameters susceptible to cause problems are modified at the end of each CFD cycle. The iterative procedure continues until the targeted turbine parameters are obtained.

This methodology based on CFD optimization process resembles to the “inverse design” method. In the inverse design method, some predefined target values are defined and imposed; optimization with the CFD validation is performed until the required value is reached [22], [36].

In this work the main target value is the runner efficiency with an adequate pressure distribution on the blades. A gradual and smooth pressure decrease on the runner blade passage is aimed. Hydraulic losses are minimized when peak pressures are avoided. The target values are reached by changing the runner geometry and runner blade angles.

2.4.3. Parametrization and Simulation of Stationary Components: Guide Vanes, Stay Vanes, Spiral Case and Draft Tube

Guide vanes and stay vanes are the other blade profiles. They are also modeled in the blade generator and analyzed in the coupled CFD code. Design of spiral case and draft tube are accomplished using standard CAD modelers.

Spiral case is created for the selected wicket gate height, runner diameter and predicted outflow angle of the spiral case. The aim is to distribute the flow uniformly around the stay vanes thus around the runner. This uniform distribution is obtained by using the theoretical “Law of constancy of the velocity moment” through the spiral case [26].

Water entering the spiral case has a moment of velocity around the rotation centerline of the runner and using this principle, the cross-sections defining the spiral can be designed to ensure evenly distributed water around wicket gate. The targeted value is the even distribution of flow and pressure along the spiral case. Spiral case is simulated separately for optimization. It is simulated with stay vanes to check the accuracy of the spiral outflow angle.

Stay vane and guide vane geometries are optimized with CFD to obtain correct flow angles and minimum hydraulic losses. The flow angles are predetermined by the runner design. Stay vane and guide vane geometries are constructed based on literature survey and experience.

Draft tube dimensions are based on the outlet diameter of the runner but also on the alignment of Francis turbine and on experience data of previous applications.

As other turbine components, draft tube is also simulated separately for the validation of the initial design. The role of the draft tube is to decrease the water velocity while increasing the pressure at the connection to tail water. Draft tube pressure recovery factor and flow behavior are investigated. Draft tube performance is described by pressure recovery factor given in equation (45).

$$C_p = \frac{P_{\text{out}} - P_{\text{in}}}{\frac{1}{2} \rho \left(\frac{Q_d}{A_{\text{in}}} \right)^2} \quad (45)$$

where C_p is the draft tube pressure recovery factor, P_{out} is the pressure at the draft tube outlet, P_{in} is the pressure at the draft tube inlet, A_{in} is the cross-sectional area of the draft tube inlet.

Apart from the turbine performance, the flow behavior inside the turbine is also important. In the design operation condition, runner outflow swirl is nearly zero; flow enters the draft tube almost vertically. The flow may separate from the solid boundaries of the draft tube inlet cone [26]. Flow separation is prevented by adjusting the inclination of the draft tube cone, represented by section H1 in Fig. 21.

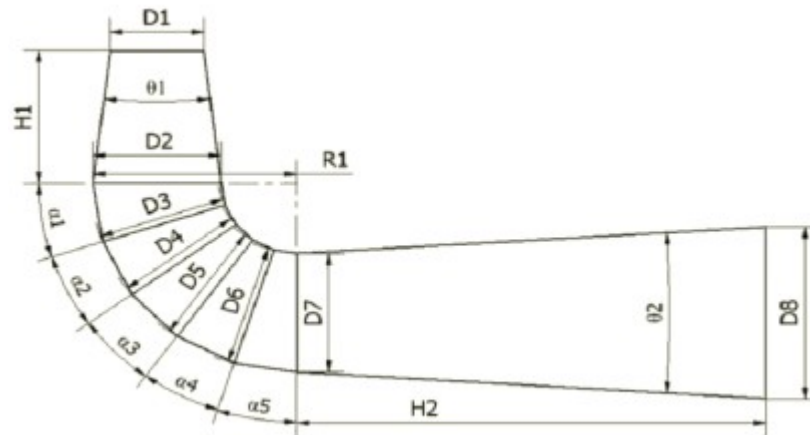


Figure 21. Parametric definition of the draft tube geometry [10]

2.4.4. Cavitation

The lifetime of a turbine runner may be shortened due to cavitation. There are different causes of cavitation in Francis turbines, such as the draft tube vortex formation, inter blade vortices or traveling bubble cavitation [31].

A leading edge cavitation may occur for unsuitable head coefficient value at the design conditions, that is when $H=H_d$ and $Q=Q_d$, [31]. Turbine head coefficient, ψ , is checked in the CFD simulations to prevent this type of cavitation.

It is essential that the runner converts most of the water energy to rotation with a smooth pressure decrease. As the runner takes the flow energy, water leaves the runner with a minimum pressure. It is important that the blade minimum pressure zones are greater than the value of the vapor pressure to avoid cavitation. The vapor pressure is calculated according to the elevation of the turbine runner: the runner minimum pressure is checked according to the calculated vapor pressure value.

In order to detect the cavitation easily, the absolute pressure definition is used throughout the simulations, such that

$$P = P_{atm} + P_{gauge} \quad (46)$$

where P_{atm} is the atmospheric pressure which is 0.1 MPa at the sea level; P_{gauge} is the gauge pressure, and P is the absolute pressure.

Atmospheric pressure can be determined according the the site elevation from the mean sea level. The following formula is proposed for the calculation of the atmospheric pressure at a specific location [26]:

$$\frac{P_{atm}}{\rho g} = 10.3 - \frac{\Delta}{900} \quad (47)$$

Here Δ is the absolute elevation; ρ is the water density (1000 kg/m³); g is the gravitational acceleration (9.81 m/s²).

Another cavitation formation is the draft tube vortex at the runner exit. It occurs at part load operation, but it only affects the turbine structural design due to vibrations [31]. This type of cavitation does not modify the runner performance at the design condition. The investigation of the draft tube vortex is therefore not included in this work.

2.4.5. Verification of Leakage

Some of the inflow is lost due to the leakage through the space between the turbine runner and stationary parts. Excessive leakage causes significant decrease in the turbine efficiency and power. The theoretically computed leakage amount is checked in CFD.

Although the leakage loss is disregarded in CFD performance simulations, the verification of leakage amount is necessary in order to determine the pressure distribution on the runner outside surface. This pressure distribution on the runner surface determines the net force on the runner in the axial direction.

Different leakage area geometry alternatives are simulated in CFD and the solution providing the best performance is chosen. In practice there are different runner profiles advised for runner sealing [13].

CHAPTER 3

CFD METHODOLOGY

3.1. CFD Analysis

Flow inside the Francis turbine is examined with CFD in 3D. It is an unsteady turbulent flow. Even though the flow inside the turbine is unsteady, steady state simulations are performed using multiple frames of reference (MFR) approach. MFR will be discussed under the mesh connection title. In this study transient simulations are avoided because of their large computational time and CPU requirements.

Ansys v.11 CFX Solver is used for the CFD analysis optimization. Turbine designers and manufacturers use widely CFX in their simulations [38], [39], [40] which proves the power and reliability of the code.

The components considered in the fluid analyses are spiral case, stay vanes, guide vanes, runner and draft tube. The simulation of the whole turbine would require very large computation time and effort. Each component is simulated separately for validation of its initial design. According to these basic simulation results, parameters are adjusted for a correct flow behavior and suitable velocity and pressure distributions.

3.1.1. Governing Equations

Navier-Stokes equations simulates the fluid motion in three dimensions. The Navier-Stokes equations can be represented as follows

$$\rho \frac{Du_i}{Dt} = \rho B_i - \frac{\partial p}{\partial x_i} + \frac{\partial}{\partial x_j} \left[\mu \left(\frac{\partial u_i}{\partial x_j} + \frac{\partial u_j}{\partial x_i} \right) + \delta_{ij} \lambda \frac{\partial u_k}{\partial x_k} \right] \quad (48)$$

Noting that the flow in question is water, and the simulation is a turbulent flow case, modifications and simplifications are made on the main equations. Governing equations of the CFD analysis program use the conservation form of Navier-Stokes equations. The conservation form of governing equations for an incompressible flow can be written in the form of

$$\begin{aligned} \rho \left(\frac{\partial u}{\partial t} + u \frac{\partial u}{\partial x} + v \frac{\partial u}{\partial y} + w \frac{\partial u}{\partial z} \right) &= \rho B_x - \frac{\partial p}{\partial x} + \mu \left(\frac{\partial^2 u}{\partial x^2} + \frac{\partial^2 u}{\partial y^2} + \frac{\partial^2 u}{\partial z^2} \right) \\ \rho \left(\frac{\partial v}{\partial t} + u \frac{\partial v}{\partial x} + v \frac{\partial v}{\partial y} + w \frac{\partial v}{\partial z} \right) &= \rho B_y - \frac{\partial p}{\partial y} + \mu \left(\frac{\partial^2 v}{\partial x^2} + \frac{\partial^2 v}{\partial y^2} + \frac{\partial^2 v}{\partial z^2} \right) \\ \rho \left(\frac{\partial w}{\partial t} + u \frac{\partial w}{\partial x} + v \frac{\partial w}{\partial y} + w \frac{\partial w}{\partial z} \right) &= \rho B_z - \frac{\partial p}{\partial z} + \mu \left(\frac{\partial^2 w}{\partial x^2} + \frac{\partial^2 w}{\partial y^2} + \frac{\partial^2 w}{\partial z^2} \right) \end{aligned} \quad (49)$$

The turbulent flow inside is simulated by Reynolds-Averaged Navier-Stokes, RANS, equations where the instantaneous variables are decomposed in mean and fluctuating values by Reynolds decomposition and these variables are time averaged

$$\begin{aligned}
\rho \frac{D\bar{u}}{Dt} &= \rho B_x - \frac{\partial \bar{p}}{\partial x} + \frac{\partial}{\partial x} \left[\mu \frac{\partial \bar{u}}{\partial x} - \rho \overline{u'^2} \right] + \frac{\partial}{\partial y} \left[\mu \frac{\partial \bar{u}}{\partial y} - \rho \overline{u'v'} \right] \\
&\quad + \frac{\partial}{\partial z} \left[\mu \frac{\partial \bar{u}}{\partial z} - \rho \overline{u'w'} \right] \\
\rho \frac{D\bar{v}}{Dt} &= \rho B_y - \frac{\partial \bar{p}}{\partial y} + \frac{\partial}{\partial x} \left[\mu \frac{\partial \bar{v}}{\partial x} - \rho \overline{u'v'} \right] + \frac{\partial}{\partial y} \left[\mu \frac{\partial \bar{v}}{\partial y} - \rho \overline{v'^2} \right] \\
&\quad + \frac{\partial}{\partial z} \left[\mu \frac{\partial \bar{v}}{\partial z} - \rho \overline{v'w'} \right] \\
\rho \frac{D\bar{w}}{Dt} &= \rho B_z - \frac{\partial \bar{p}}{\partial z} + \frac{\partial}{\partial x} \left[\mu \frac{\partial \bar{w}}{\partial x} - \rho \overline{u'w'} \right] + \frac{\partial}{\partial y} \left[\mu \frac{\partial \bar{w}}{\partial y} - \rho \overline{v'w'} \right] \\
&\quad + \frac{\partial}{\partial z} \left[\mu \frac{\partial \bar{w}}{\partial z} - \rho \overline{w'^2} \right]
\end{aligned} \tag{50}$$

3.1.2. Turbulence Models

Different turbulence models are used with RANS equations. In this work two equations models are preferred, namely k- ϵ and SST models.

The mainly used turbulence model in the simulations is the standard k- ϵ model. Although it is known that k- ϵ is not always sufficient in the modeling of turbulent flow [22], it is widely used in the turbine design and optimization applications [39], [40]. This method accounts for the turbulence eddy dissipation which is the rate at which velocity fluctuations dissipate. Besides high quality mesh is constructed, CFD code provides scalable wall functions.

Another turbulence model in question is the Shear Stress Transport (SST) model. The same automatic wall treatment is valid. SST is suggested to obtain good results of flow separation predictions [42]. Use of SST is only performed for runner simulation.

3.1.3. Advection Schemes

Different advection scheme options are used throughout the simulations namely upwind, high order upwind and high resolution.

Faster simulations for the determination of overall geometry of components are performed using coarser mesh. For the runner, in order to reduce the design time span, initial simulations are performed with coarse mesh and upwinding scheme in k- ϵ turbulence model. For fine mesh simulations k- ϵ and shear stress transport methods are used as turbulence models to see the effect on the flow separation at the runner, as advised. A high resolution advection scheme is selected for fine mesh cases.

3.1.4. Discretization Scheme

Finite volume method is used for the discretization of the flow region. The flow region is subdivided into small control volumes in which the mass and momentum are conserved.

3.1.5. Mesh Connection

A steady state approach for runner simulations is possible due to the MRF concept. In this concept, each component domain is independent. Stationary frame of reference is assigned to stator parts. Rotational frame of reference is assigned to the runner defining its rotational speed. This method requires the interface to be uniform. Within this concept there are two possible mesh connection methods:

- GGI (General grid interface) is used when the grid on either side of the connecting surface does not match: an interpolation of results is performed; this interpolation result is used as input for the following mesh. This option

is preferred to connect two regions such as “Spiral case + Stay vanes”, “Stay vanes + Guide vanes” where all the regions are stationary.

- In the frozen rotor approach, coordinate transformation is made from rotating to stationary, averaged values are mapped on a stationary frame. Using the MFR approach, an unsteady problem can be solved as a steady case; this method gives good results [41]. The frozen rotor option is used to connect two regions such as “Guide vanes + Runner”, “Runner + Draft tube” where the runner is rotating and others are stationary.

3.1.6. Boundary Conditions

Pressure inlet and mass flow outlet conditions are used for runner simulations, as advised for rotating components of turbomachinery simulations [42]. Solid boundaries are given non slip condition.

The hydraulic efficiency of the spiral case, stay vanes and guide vanes are taken into account in the computation of the runner inlet pressure. All the hydraulic losses from the spiral inlet until the runner inlet is extracted from the net head of the turbine. The resulting net head available for the runner is then assigned as the pressure inlet condition for the runner simulation.

As mentioned in the methodology section, some assumptions are made for the simulations such as the negotiation of the leakage through the runner and the roughness of the runner blades. A mass flow of 2 m³/s is therefore selected as the outlet boundary condition. The leakage loss is not considerable compared to turbine overall efficiency. However the roughness height of the blades alters the efficiency; the results are presented in Chapter 5.

CFD analysis is performed for spiral case with mass flow rate given as inlet boundary condition. CFD results indicate the necessary adjustments in spiral case

geometry to obtain evenly distributed flow over the radial outlet section of the spiral. Modifications of spiral cross sections are also necessary to obtain the required flow angle at the spiral exit in order to prevent improper angle of attack to stay vanes.

Guide vane and stay vane positions are adjusted based on the CFD results. Exact inflow and outflow angles through stay and guide vanes leads to the computed inflow angle to turbine runner.

The outflow condition of the runner is obtained from CFD and transferred to the draft tube simulations as inlet condition.

3.2. Grid Generation

3.2.1. Topology Definition

A high quality mesh is required for blade profiles. This can be accomplished by defining accurate topology geometries around the blade. Different topology like H/ J/L/C grids & O grids are used to satisfy the optimum face angles (Fig. 22).

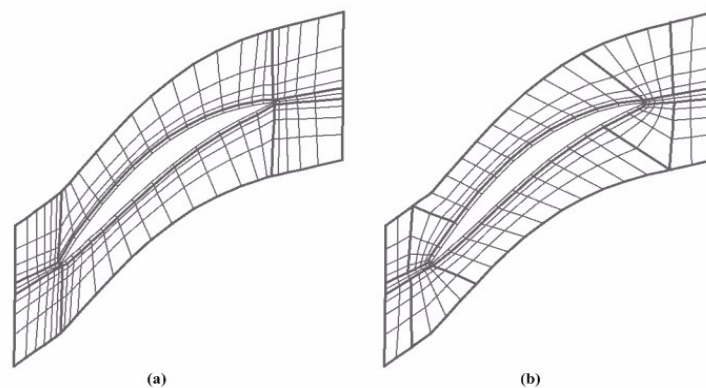


Figure 22. (a) H-grid type topology (b) J-grid type topology

In the simulated turbine, all the blade profiles are meshed using a mixed topology. This topology includes an O-grid forming loop around the blade profile. This option is very useful in solving the boundary layer. In this simulation the thickness of the O-grid elements are defined with a width factor of 0.2 i.e. the O-grid thickness is 0.2 times the average blade width. Near wall element size, i.e. the spacing between the wall layer and the first node layer, can be defined by three methods: “ y^+ ”, “Normalized” or “Absolute”. In this simulation the normalized option is selected. Normalization is interpreted as the absolute distance divided by the maximum possible distance. The latter is one of the following, as appropriate: boundary layer thickness, distance from hub to shroud/tip, thickness of the O-Grid, distance from the shroud to the tip. In fact the y^+ value does not affect the convergence of the solution in this work because either k- ϵ or SST models are used with automatic wall functions.

3.2.2. Mesh Generation

The blade profiles are meshed in *TurboGrid* which is coupled to the blade generator tool. Using the predefined topology selection a high quality structured mesh is obtained for runner blades, stay vanes and guide vanes, as illustrated in Fig. 23. The minimum angular resolution is 15 degrees and maximum 165 degrees for the mesh faces.

Meshes for other components (Spiral case, draft tube) are generated in *CFX-Mesh* which uses unstructured mesh definition. A minimum angular face resolution of 18 degrees is applied. Mesh clustering is applied towards the connection areas, in order to have a good grid connection between fine blade meshes and coarser hexa meshes. For example for the spiral case, the mesh size is smaller at the spiral outlet as illustrated in Fig. 24.

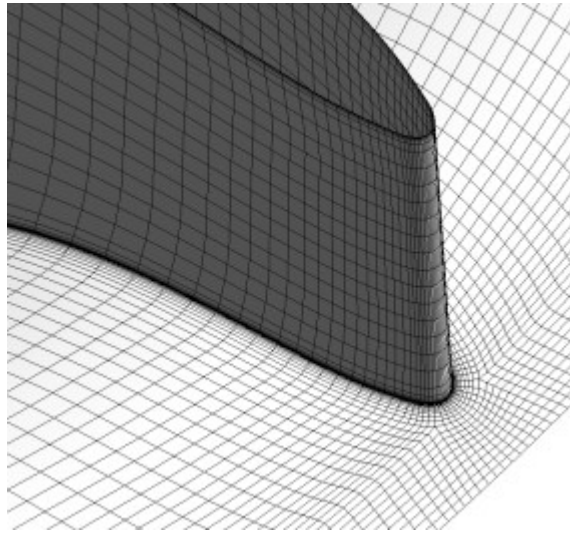


Figure 23. Generated mesh layout on the runner blade leading edge

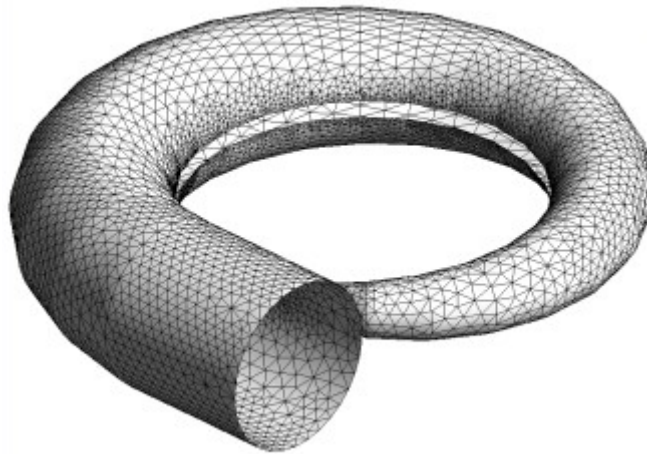


Figure 24. Hexahedral mesh of the spiral case

CHAPTER 4

APPLICATIONS

4.1. Project Specifications

4.1.1. Definition of the Problem

The methodology developed is applied for the design of turbines of a hydropower project in Turkey. This small-medium scale hydropower project is under realization stage. The hydropower plant is named Cuniş. It is located in Rize, north of Turkey, in the Black Sea region. Three identical Horizontal Francis type turbines are required by the project owner. The plant installed capacity is approximately 9 MW.

4.1.2. Input Values

Necessary input variables are the net head and the system discharge. Cuniş hydropower plant is a run-of-river type project having a net head of 164.84 m and a total design discharge of 6 m³/s. Three turbines of the same type and having the same properties are required by the project owner and the designer. The design head and discharge are therefore 164.84 m and 2 m³/s per turbine while three turbines are in operation. A maximum net head of 168.08 m is available while only one turbine operates with 2 m³/s. Design head and discharge values indicate the suitability of horizontal shaft Francis type turbines based on turbine selection charts.

4.2. Sample Runner Design Procedure

4.2.1. Turbine power

Considering the design head of $H_d = 164.84\text{ m}$ and a design discharge of $Q_d = 2.0\text{ m}^3/\text{s}$, a Francis type turbine is selected for the design referring to Fig. 3.

Turbine efficiency is determined based on the project requirements: High efficiencies are difficult to reach for small hydro projects because the friction losses increase for decreasing turbine dimensions. In large scale projects producing hundreds of megawatts of powers, turbine efficiency can reach 94 %. In small and medium scale projects, the effect of friction losses inside the turbine is comparatively high. A small hydropower project implies a power plant producing power up to 1 MW. Low efficiencies are therefore acceptable depending on the project scale. Time restriction is also another factor on determining the targeted efficiency; a longer and more detailed simulation process is necessary to obtain an optimized turbine geometry yielding higher efficiency. In this work an overall turbine efficiency of $\eta = 0.91$ is aimed. Despite such an efficiency rate appears to be slightly low for a Francis turbine, it is adequate for this medium scale project and meets the requirements of the project owner. The power of the turbine is therefore calculated as:

$$P_d = \rho g Q_d H_d \eta = 2943\text{ kW}$$

and in horsepower:

$$P_{hp} = \frac{P_d}{0.7355} = 4001\text{ hp}$$

4.2.2. Turbine speed

Using the procedure given in 2.3.3. , the rotational speed is calculated.

$$c_{nq} = \min(2600; 2600 - (200000 - P_d)/365) = 2060.11$$

$$n_q = \frac{c_{nq}}{H_d^{0.535}} = 134.20$$

$$n = n_q \frac{H_d^{1.25}}{P_d^{0.5}} = 1453 \text{ rpm}$$

According to the power value, the rotational speed is directly calculated as 1453 rpm. This speed is not a synchronized value. First the pole number should be is determined:

$$\text{number of pole pairs} = \frac{f \cdot 60}{n} = \frac{(50)(60)}{1453} = 2.06$$

This pole pair number is rounded up to 3. Turbine rotational speed is then calculated using equation (8):

$$n = n_{sync} = \frac{120 * f}{2 * (\text{number of pole pairs})} = \frac{120 * 50}{2 * 3} = 1000 \text{ rpm}$$

The angular rotational speed of the runner is:

$$\omega = 2\pi \frac{n}{60} = 104.72 \text{ rad/s}$$

4.2.3. Specific Speed

The specific speed of the turbine is calculated using equations (9) and (10):

$$n_s = n_{sync} \frac{P_d^{0.5}}{H_d^{1.25}} = 1000 \frac{(4045)^{0.5}}{(164.84)^{1.25}} = 108.3$$

and

$$n_q = n \frac{\sqrt{Q}}{H^{3/4}} = 1000 \frac{\sqrt{2.0}}{164.84^{(3/4)}} = 32.5$$

4.2.4. Determination of Preliminary Runner Dimensions

Runner preliminary dimensions are obtained from the experimental curves as follows:

- Shaft diameter: $D_s = 154 \text{ mm}$
- Runner inlet diameter: $D_1 = 710 \text{ mm}$
- Runner throat diameter: $D_2' = 518 \text{ mm}$
- Runner outlet diameter: $D_2 = 518 \text{ mm}$
- Runner height: $b_1 = 174 \text{ mm}$
- Wicket gate height: $b_0 = 80 \text{ mm}$
- Wicket gate diameter: $D_g = 855 \text{ mm}$

The preliminary meridional shape of the runner is illustrated in Fig. 25. The specific speed of 108.3 of the turbine indicates a low speed Francis runner. The meridional shape should resemble the one with $n_s=80$ as was illustrated in Fig. 9. The obtained runner in Fig. 25 satisfies the expectation of a low specific speed runner.

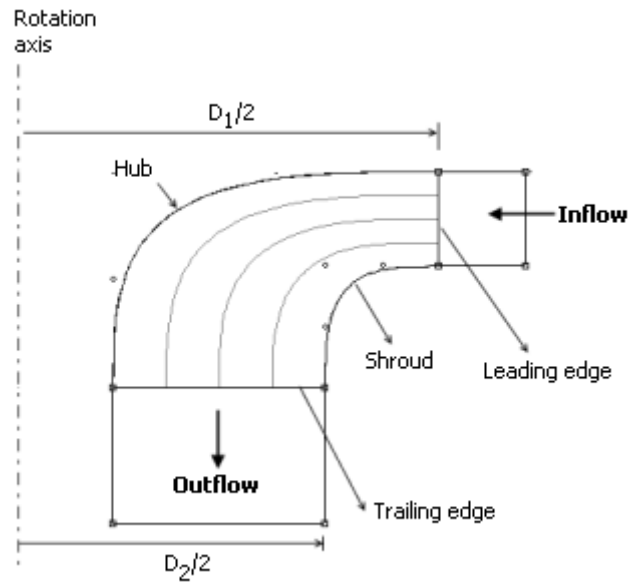


Figure 25. Meridional representation of the runner preliminary dimensions

4.2.5. Determination of the Exit Diameter

The preliminary runner shape is determined based on experimental data. This shape will be used as a guidance throughout the design. However, it is necessary to determine final runner shape by using other theoretical formulas.

Petermann [29] proposes the computation of flow exit velocity for the determination of the runner shape. First meridional flow velocity at the runner exit is calculated using equation (42):

$$v_{2m} = \sqrt{2gH_d \varepsilon} = 10.318 \text{ m/s}$$

where the variable ε is calculated by the following equation

$$\varepsilon^2 = 1.16 * 10^{-3} \left(\frac{\delta_r n_q}{\sqrt{k}} \tan \beta \right)^{4/3} \quad (51)$$

in which the variables are selected as $\delta_r = 1$, $k = 1$, $\beta = 24.5^\circ$ for the Francis turbine of specific speed $n_q = 32.5$ [29]. Exit area of the runner can be defined as $A_2 = Q_d/v_{2m}$. The area can be roughly calculated as $A_2 = \pi D_2^2/4$. The exit diameter is:

$$D_2 = \sqrt{(4Q_d)/(\pi v_{2m})} = 491 \text{ mm}$$

4.2.6. Determination of the Inlet Diameter and Throat Diameter

The inlet velocity is related to the outflow velocity by equation (43), where a is taken equal to “1” for $n_q < 70$ [29]. The inlet radial (or meridional) velocity is obtained as (Fig. 26):

$$v_{1m} = (1)v_{2m} = 10.318 \text{ m/s}$$

The inlet circumferential velocity is calculated by equation (44).

$$u_1 = \frac{v_{1m}}{2 \tan \beta_1} + \sqrt{\left(\frac{v_{1m}}{2 \tan \beta_1}\right)^2 + gH_d \eta} = 39 \text{ m/s}$$

The inlet diameter at point i_5 is derived as:

$$D_1(i_5) = 2u_1/\omega = 745 \text{ mm}$$

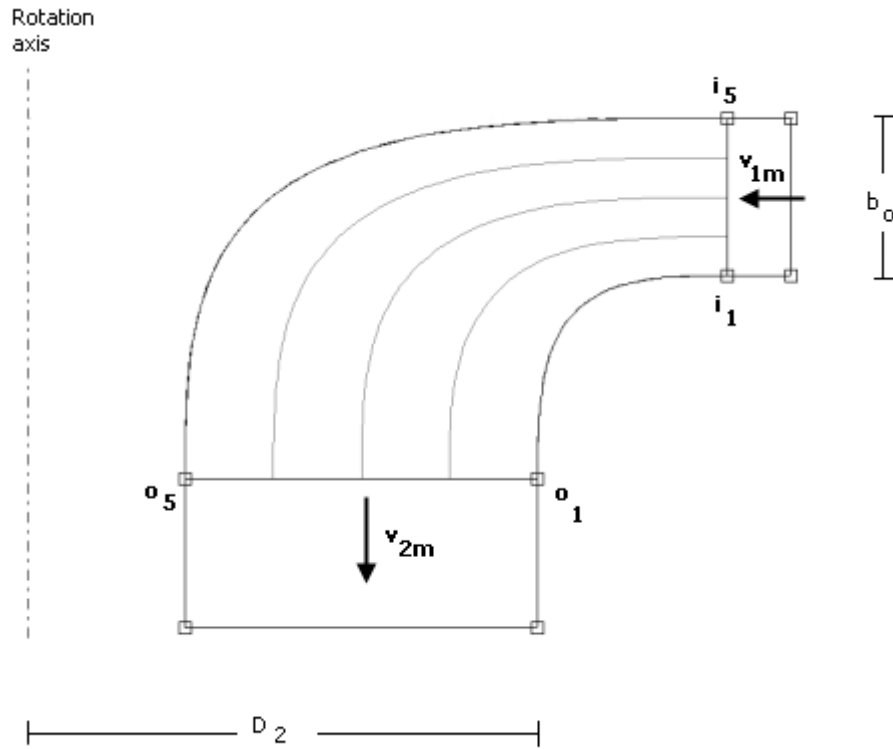


Figure 26. Meridional profile definition points

The condition that “ $D_1(i_5) > D_2$ ” implies that the runner inlet diameter is constant on leading edge:

$$D_1(i_5) = D_1(i_1) = D_1 = 745 \text{ mm}$$

4.2.7. Determination of the Wicket Gate Height

As the turbine dimensions are determined and the design inlet velocity is decided, wicket gate height b_0 is obtained from the basic equation “ $Q_d = A_1 v_{1m}$ ” where A_1 is the runner inlet area and v_{1m} is the meridional inlet velocity:

$$A_1 = (\pi D_1) b_0$$

$$b_0 = Q_d / (\pi D_1 v_{1m}) = 82 \text{ mm}$$

4.2.8. Determination of the Optimum Guide Vane Flow Angle

Water energy decreases in the runner: the circulation value decreases through the blade passage and water leaves the runner with minimum energy. A maximum performance is expected from the runner at its design operation point. The maximum energy can be extracted by the turbine runner if the values of outlet circulation Γ_2 is at its minimum value near zero, as implied by the equation (40). The circulation at the runner outlet is by definition

$$\Gamma_2 = (\pi D_2) v_2 \cos(\alpha_2) \quad (52)$$

A zero outlet swirl leads to an outflow angle of $\alpha_2 = 90^\circ$ for the operating point. This demonstration is in accordance with the statement proposed by Raabe [13]: *“In most of the hydro turbines, the moment of momentum of flow upstream of the runner is nearly constant. This follows from the intention, to extract from any stream tube the same available specific energy, namely head by means of the theorem of moment of momentum under the assumption of a whirl-free outlet which usually occurs at least at the best efficiency point.”*

The outlet swirl is considered zero at the design operation condition, under the design head and design discharge values. In this case the Euler equation reduces to:

$$H_d \eta = \Gamma_1 \omega / g 2 \pi \quad (53)$$

It was demonstrated that the circulation is conserved between the guide vanes and the runner inlet. Therefore,

$$\Gamma_0 = H_d \eta g 2\pi / \omega = 88.292 \quad (54)$$

As the magnitude of circulation is known, the circumferential velocity at the guide vane exit can be computed from the definition of circulation:

$$\Gamma_0 = (\pi D_0) v_0 \cos(\alpha_0) = (\pi D_0) v_{0u} \quad (55)$$

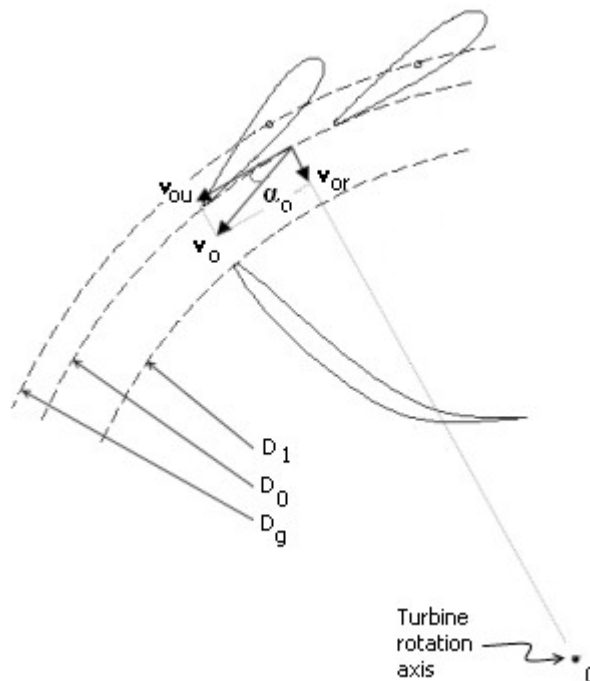


Figure 27. Guide vane exit flow velocities

The guide vane exit diameter is selected as $D_0 = 775 \text{ mm}$ at the design operation condition. Circumferential velocity at the guide vane exit is calculated using equation (55):

$$v_{0u} = \frac{\Gamma_0}{\pi D_0} = 36.264 \text{ m/s} \quad (56)$$

Radial velocity at the guide vane exit is calculated as follows:

$$v_{0m} = v_{0r} = \frac{Q}{\pi D_0 b_0} = 10.018 \text{ m/s} \quad (57)$$

Circumferential and radial velocity components indicate the optimum guide vane exit angle as: $\alpha_o = 15.44^\circ$

4.2.9. Assignment of the Blade Profile

The final dimensions are very close to the initial assumption. Final dimensions of the blade meridional profile are determined as shown in Fig. 28. Leading and trailing edge profiles are determined using spline control points. Hub and shroud curves are manipulated using Bézier control points.

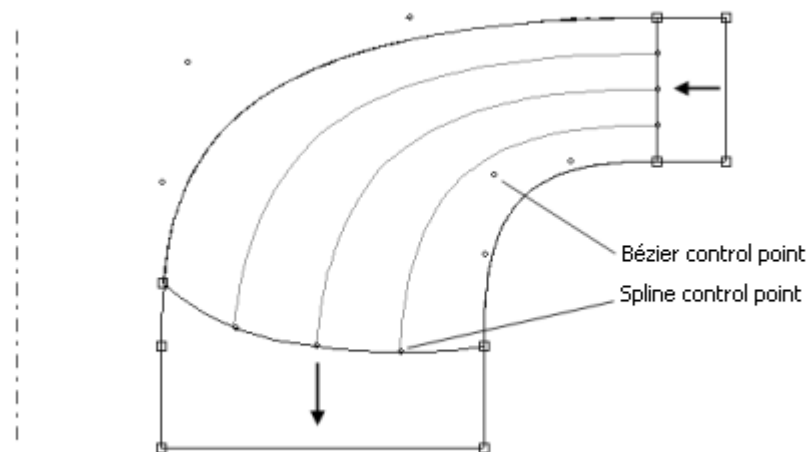


Figure 28. Meridional profile determined by experience and the control points

4.2.10. Determination of the Inlet Velocity Triangles and Blade Angles

For demonstration purpose, all the calculations are made for midpoints i_3 and o_3 , of the leading edge and the trailing edge to simplify calculations.

Inlet circumferential velocity is computed from the circulation value:

$$\Gamma_1 = \pi v_{1u} D_1$$

$$\Gamma_0 = \Gamma_1$$

$$v_{1u} = \Gamma_0 / (\pi D_1) = 37.72 \text{ m/s}$$

The radial (or meridional) velocity at the inlet is computed from discharge:

$$v_{1m} = Q_d / (\pi D_1 b_o) = 10.42 \text{ m/s}$$

Total inflow velocity and the inflow angle are:

$$v_1 = 41.09 \text{ m/s}$$

$$\alpha_1 = 15.44^\circ$$

Circumferential velocity at the blade inlet point i_3 is:

$$u_1(i_3) = D_1 \omega / 2 = 39.00 \text{ m/s}$$

From trigonometry the relative velocity of water and the relative flow angle are:

$$w_1 = 10.50 \text{ m/s}$$

$$\beta_1 = 83.00^\circ$$

A shock free entrance is only possible when the relative flow angle is equal to the blade angle. The blade angle is therefore:

$$\delta_1 = \beta_1 = 83.00^\circ$$

Velocity triangles and angles are illustrated in Fig. 29.

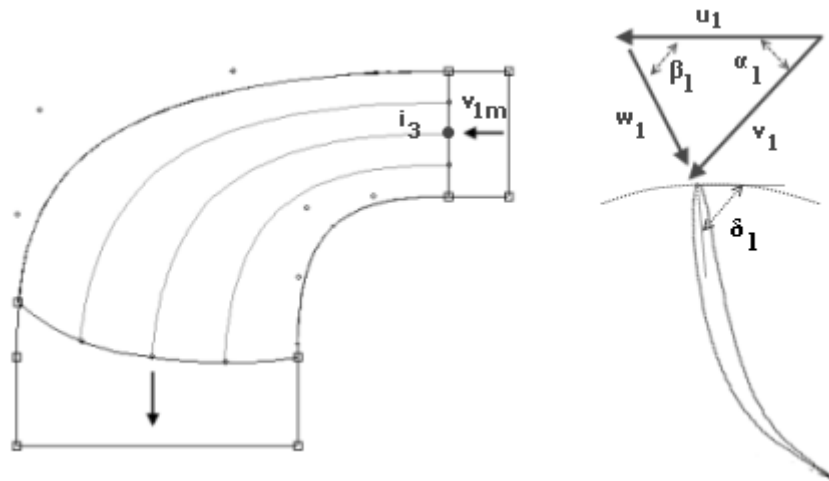


Figure 29. Blade inlet velocity triangles

4.2.11. Determination of the Exit Velocity Triangles and Blade Angles

At the runner exit water should not have circumferential component for the maximum efficiency. Based on this assumption the outlet flow angles is: $\alpha_2 = 90^\circ$
The outflow circumferential velocity is therefore:

$$v_{2u} = 0$$

Outlet area A_2 is retrieved from the blade generator; the outflow angle is:

$$v_2 = v_{2r} = Q_d/A_2 = 12.35 \text{ m/s}$$

Circumferential velocity at the outlet is point o_3 is:

$$u_2 = D_2(o_3)\omega = 17.38$$

From trigonometry the relative velocity of water and the relative flow angle are:

$$w_2 = 21.32 \text{ m/s}$$

$$\beta_2 = 35.40^\circ$$

The blade angle is taken equal to the relative flow angle to prevent any separation and vortices at the blade exit. The blade angle is therefore:

$$\delta_2 = \beta_2 = 35.40^\circ$$

Flow angles and velocity triangles are illustrated in Fig. 30.

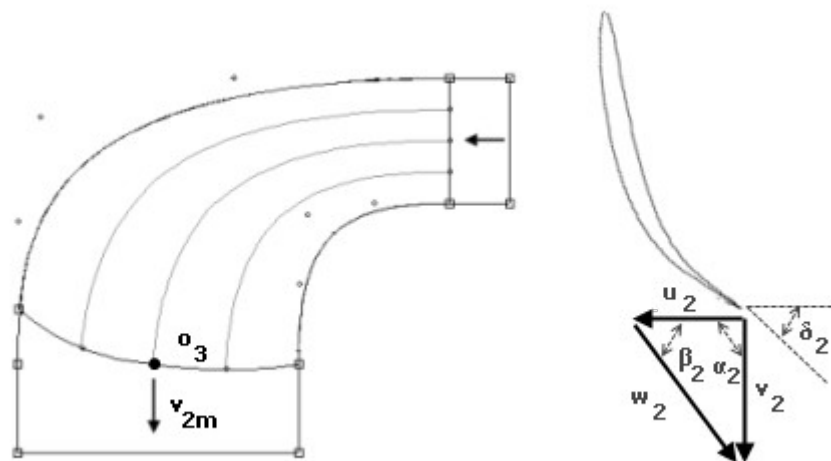


Figure 30. Blade outlet velocity triangles

4.2.12. Blade Shape Transferred to CFD Simulation

Blade generator provides new corrected inflow and outflow areas for different blade angles, as shown in Fig. 31. After each blade angle definition, “corrected flow area” changes slightly. Iterations between the corrected area and the blade angle are repeated until obtaining no change in the corrected area. At this stage the correct blade angles are obtained. The reason of such a modification is that the first runner design is based on the midpoints of the leading and trailing edges of the blade. The design is performed on the midsection for simplicity. However the flow conditions (flow areas) are not identical going from hub to shroud on the same blade edge.

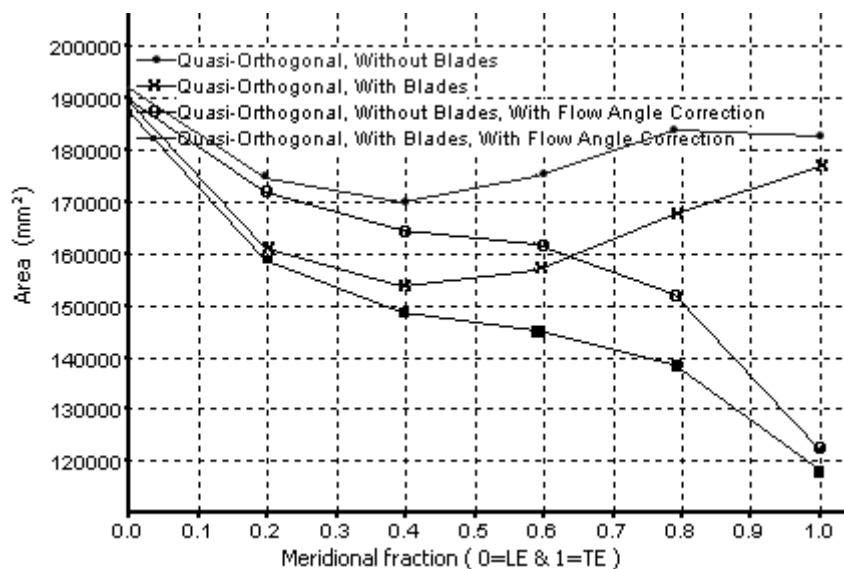


Figure 31. Change of flow area through the blade passage

Blade generator generates the flow nets and they can be manually adjusted by control points, as shown in Fig. 32. The hub and the shroud profile are then adjusted according to the flow nets and by literature survey.

The flow region is mapped to meridional section plane. Blade thickness profile is

defined for each meridional section, as shown in Fig. 33. Symmetrical NACA airfoil profile, such as NACA 0010, is defined for each meridional cross section [32].

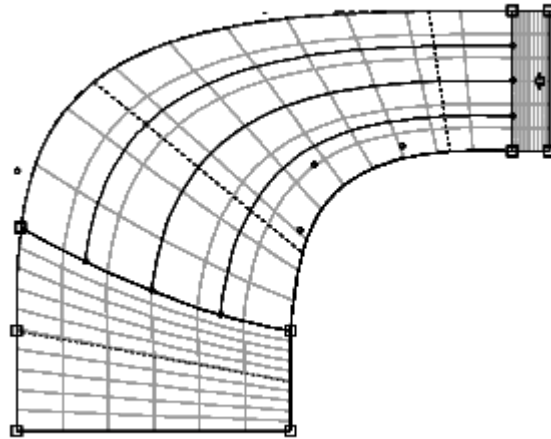


Figure 32. Flow nets generated by the program

Inlet and outlet flow conditions and angles are provided by Euler equations. Distribution of blade angles for each meridional section is defined by B-spline curves and final blade design takes the form in Fig. 34. This profile is subject to modification after CFD results to obtain a smooth pressure decrease on the blade.

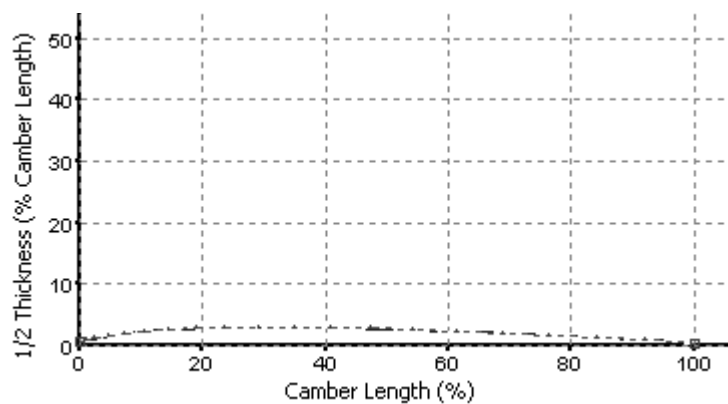


Figure 33. Blade thickness profile for the first test case

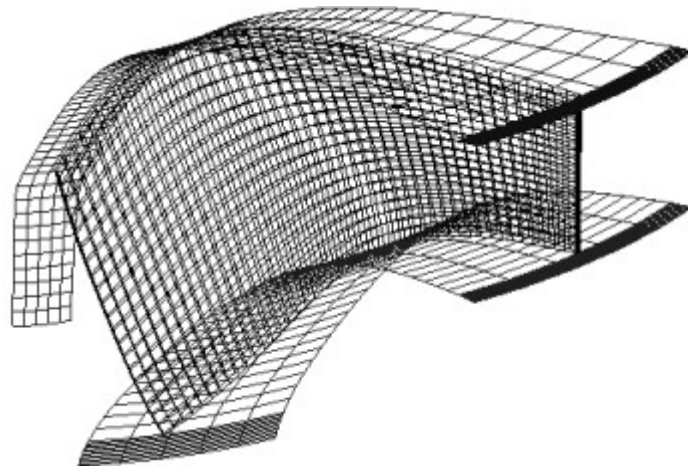


Figure 34. Blade flow passage

4.3. CFD Simulations

4.3.1. Summary of the CFD optimization procedure

As mentioned in the CFD methodology chapter, the commercial code CFX of ANSYS is used for CFD analysis. For first rapid optimization stage coarser mesh sizes are used. In the second stage small changes are made on turbine parameters line blade angles. A fine mesh resolution is therefore needed in the second stage. Different turbulence models and advection schemes are used depending on the mesh size available. A summary of the CFD optimization procedure is tabulated in Fig. 35.

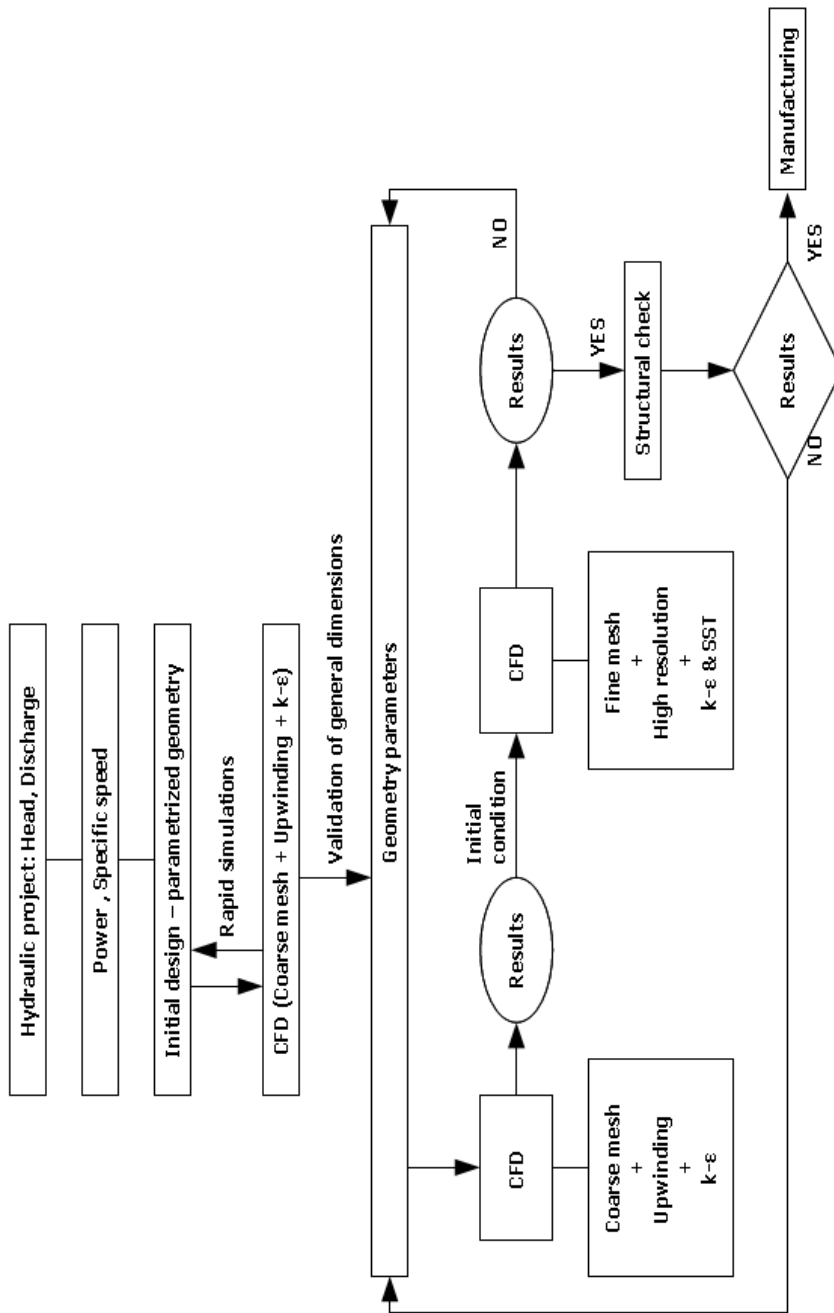


Figure 35. Summary of the CFD optimization procedure

4.3.2. Generated Mesh Data for the Final Design

The mesh properties in the designation of the final design are listed in Table 3.

Table 3. Mesh characteristics of each turbine component for final design

Component	Mesh type	Number of elements	Number of nodes
Spiral case	Tetrahedral	209602	40152
Stay vane	Hexahedral	240000 (x 12 blades)	256680
Guide vane	Hexahedral	240912 (x 24 blades)	254560
Runner blade	Hexahedral	238560 (x 15 blades)	255200
Draft tube	Tetrahedral	290224	23392

CHAPTER 5

RESULTS

5.1. Runner Simulations

More than 100 trial blade designs are accomplished. Design cases are simulated in CFD for the runner optimization. Each design case has actually more than 20 parameters to be defined. However, an automatized optimization method is not established; it would be another research area in itself. All the results and parameters are therefore not presented. Only the targeted and major parameters are listed.

Design-optimization procedure consists of two stages. In the first stage overall runner dimensions are decided to fit the project requirements. Main target values are the runner efficiency and runner shaft power. Simulations of the first stage are realized using coarser mesh size, to benefit from computational effort. A coarse mesh simulation does not provide the exact solution; but it permits the comparison of different test cases. Selected cases of first stage are listed in Table 4.

After determining the overall dimensions, fine adjustments are needed to reach the target values. In stage 2, mainly the blade δ angles are adjusted. Fine mesh resolution is used in stage 2, in order to catch accurately the effect of small angle variations. Selected cases of the second stage are listed in Table 5. In the above stages, a coarse mesh resolution implies approximately 3×10^4 elements per 1 blade; a fine mesh resolution implies approximately 25×10^4 elements per 1 blade.

Table 4. Parameters of the selected cases for stage 1

Parameters	Case 1	Case 2	Case 3	Case 4	Case 5	Case 6	Case 7	Case 8	
Design	D_1	745	745	745	745	788	788	788	
	D_2	491	491	491	491	516	516	516	
	b_o	82	82	82	82	60	60	60	
	b_1	185	185	185	185	137	137	137	
Profile	NACA0006	NACA0006	NACA0012	NACA0008	NACA0006	NACA0006	NACA0006	NACA0010	
α_o	14.39	15.00	14.39	14.39	13.16	19.89	20.39	20.39	
θ	30.00	30.00	30.00	30.00	42.00	48.00	48.00	48.00	
CFD Result	η	94.67	95.04	94.58	94.35	94.79	95.32	95.45	94.58
	P	2.867	2.727	2.873	2.859	3.082	3.057	2.989	2.98
	ϕ	0.4618	0.4618	0.4602	0.4593	0.4189	0.3081	0.3307	0.3310
	ψ	1.1524	1.0918	1.1534	1.1491	1.1598	0.9770	0.9538	0.9606

Table 5. Parameters of the selected cases for stage 2

Parameters		Case 9	Case 10	Case 11	Case 12	
Design	D_1	788	788	788	788	mm
	D_2	516	516	498	498	mm
	D (at point o_5)	238	238	294	294	mm
	b_o	60	60	60	60	mm
	b_1	137	137	169	169	mm
	Profile	NACA0010	NACA0010	NACA0010	NACA0010	
	α_o	20.39	20.39	20.39	20.39	degree
	θ	48.00	48.00	48.00	48.00	degree
	β (at LE point i_1)	70.00	90.00	90.00	90.00	degree
	β (at LE point i_2)	70.00	90.00	90.00	90.00	degree
	β (at LE point i_3)	70.00	90.00	90.00	90.00	degree
	β (at LE point i_4)	70.00	90.00	90.00	90.00	degree
	β (at LE point i_5)	70.00	90.00	90.00	90.00	degree
	β (at TE point o_1)	22.18	5.77	26.90	22.78	degree
	β (at TE point o_2)	25.68	15.93	19.50	23.26	degree
	β (at TE point o_3)	29.97	28.28	23.87	26.52	degree
	β (at TE point o_4)	35.31	33.45	27.41	29.63	degree
β (at TE point o_5)	41.56	39.28	35.11	31.76	degree	
CFD Results	η_t	97.71	97.30	97.44	97.45	
	P	2.935	3.203	2.995	2.963	MW
	φ	0.3312	0.3319	0.3384	0.3385	
	ψ	0.9157	1.0049	0.9503	0.9404	
	α_1	20.37	20.37	20.37	20.37	degree
	α_2	83.74	60.43	88.48	86.39	degree
	P_{min}	< P vapour	< P vapour	< P vapour	> P vapour	
LE shock entrance	Yes	No	No	No		

5.1.1. Optimization of Meridional Profile

Different meridional shapes are simulated, the hub and shroud profile modification leads to higher runner performance. Case 6 has a higher efficiency than the Case 5, the blade shapes are illustrated in Fig. 36.

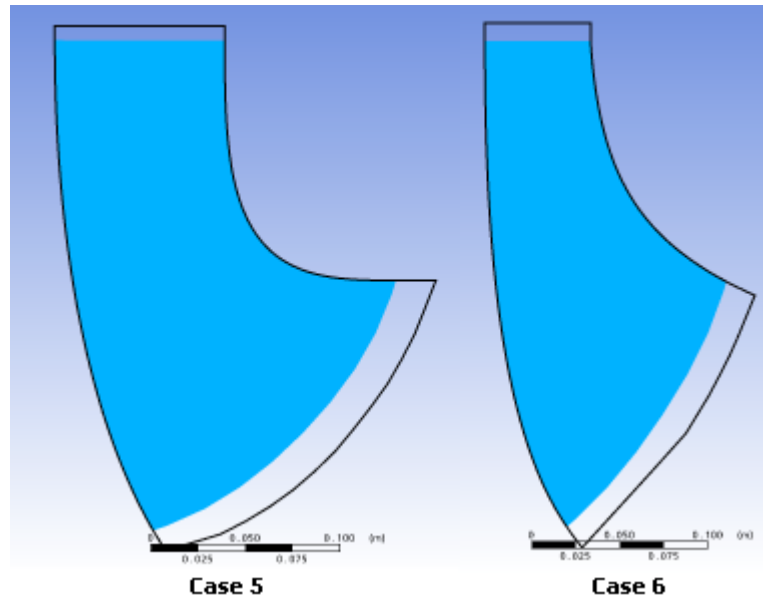


Figure 36. Runner blade meridional shapes for Case 5 and Case 6

5.1.2. Leading Edge Shock Free Entrance

A leading edge shock can be easily detected by plotting the pressure distribution on the runner blade section, and by examining the velocity vectors in the flow passage.

Wrong inflow angles at the runner inlet may cause flow separation at the blade suction side. In order to prevent this phenomenon, a shock-free entrance should be ensured for the design operational case.

In Case 9, a peak pressure occurs at the blade leading edge, as seen in Fig. 37. By changing the blade angle at the blade leading edge, this peak pressure is eliminated and a smooth distribution is obtained as shown in Fig. 38.

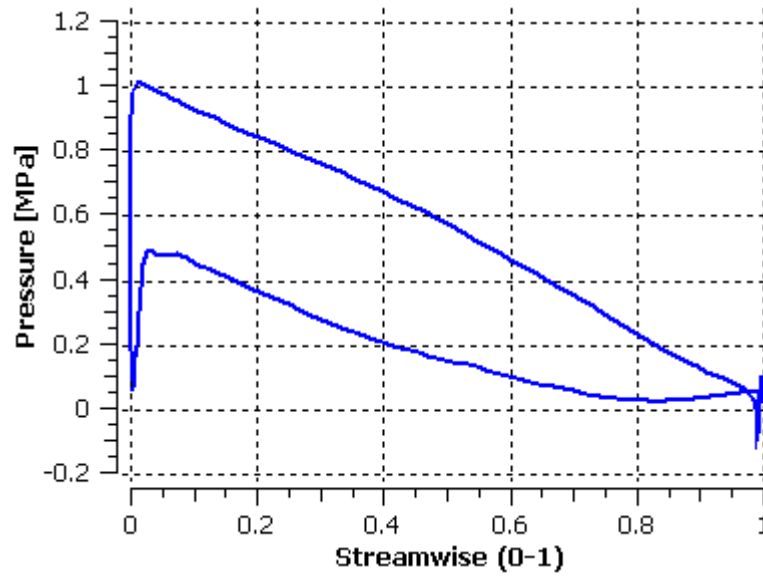


Figure 37. Case 9 - Pressure on the blade meridional section i_3-o_3

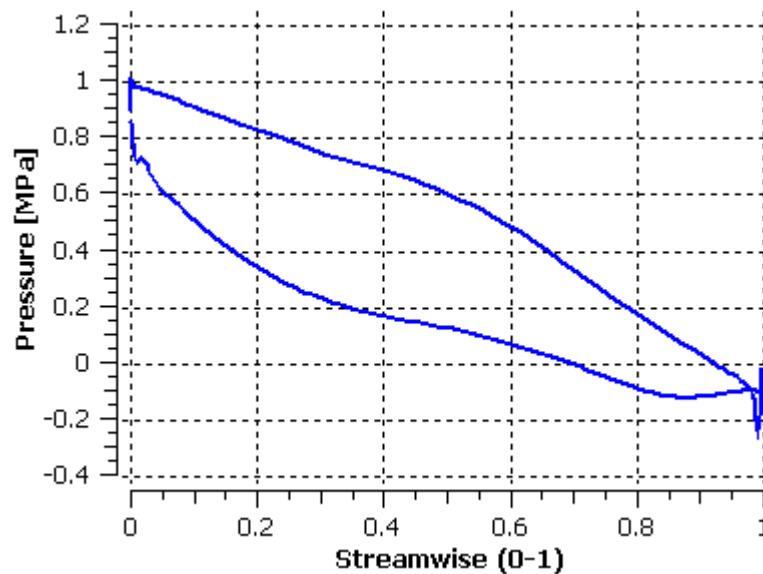


Figure 38. Case 10 - Pressure on the blade meridional section i_3-o_3

In Case 9, the exit flow velocity is not as high as expected and the velocity vectors are not following the blade orientation as shown in Fig. 39. This is an indication of wrong blade angle distribution. In Case 10 the blade trailing edge angles are modified. This modification lead to the change of net flow are between the blades and the change in the flow velocity and velocity vector orientations, as shown in Fig. 40.

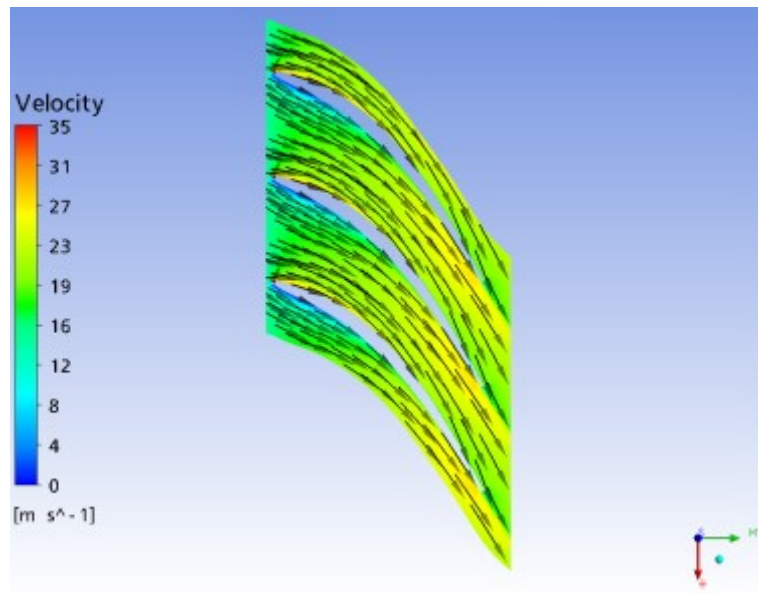


Figure 39. Case 9 - Velocity vectors for meridional section i3-03

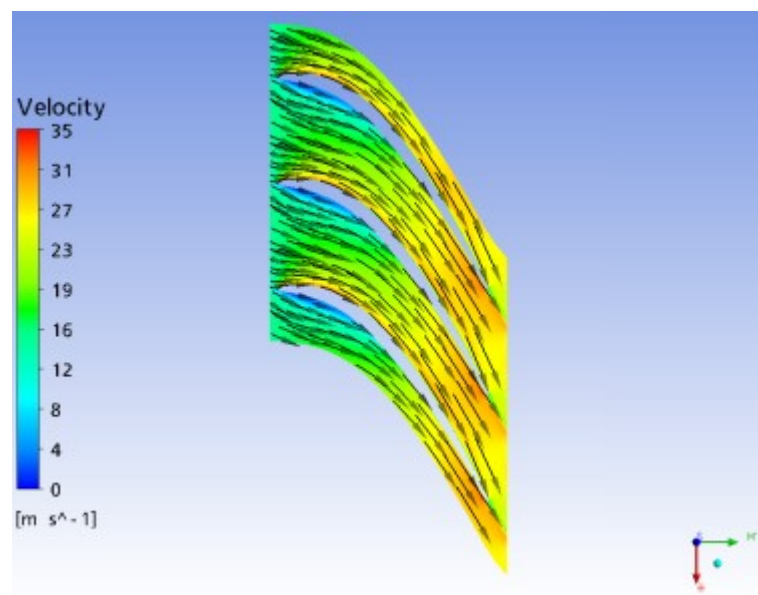


Figure 40. Case 10 - Velocity vectors for meridional section i3-03

5.1.3. Outlet Swirl

An outlet swirl indicates an improper blade angle at the trailing edge. Trailing edge angle of the blade is modified based on the flow angle output of the CFD simulation. As shown in Table 5, CFD simulations provide the outflow angle is nearly 90 degrees, indicating an almost vertical exit flow velocity. The circulation at the outlet is nearly zero; which is compatible to the initial assumptions.

5.1.4. Prevention of Cavitation

The pressure contours on the blade surface are plotted for the Case 12 as in Fig. 41. The pressure decreases and a minimum pressure zone occurs on the blade suction side near the shroud.

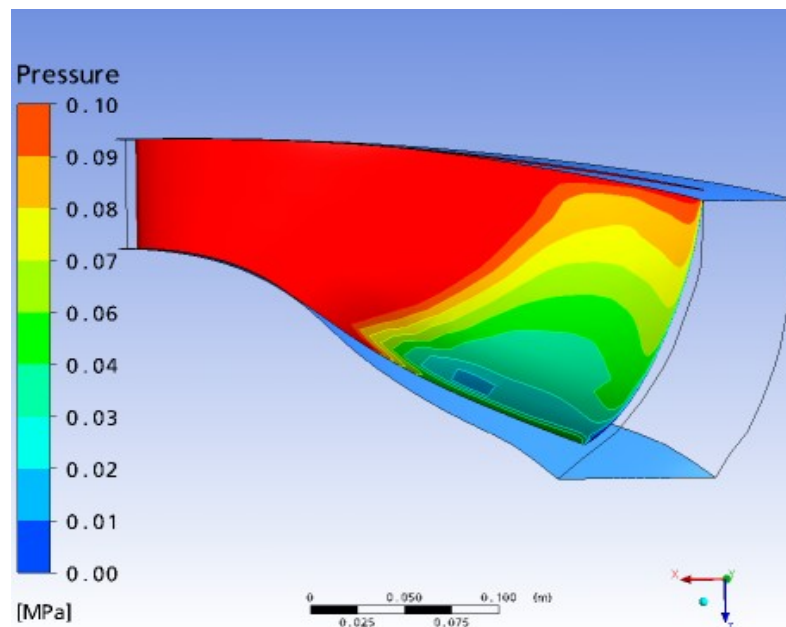


Figure 41. Pressure distribution on blade suction side for Case 12

The water vapor pressure is approximately calculated as 0.02 MPa. As indicated by Fig. 42, the minimum pressure on the blade is higher than the vapor pressure for the final case, Case 12. Cavitation on blade suction side is therefore eliminated.

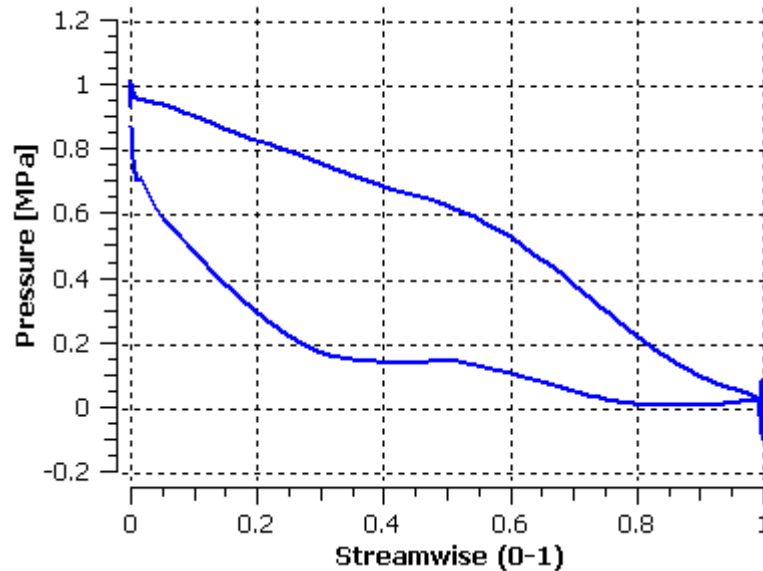


Figure 42. Case 12 - Pressure on the blade meridional section with minimum pressure zone

The head coefficient ψ of Case 12 is obtained as 0.9404. The head coefficient should be between 0.9 and 1.0 for a good turbine performance. The last design is therefore within the required limits. The turbine runner should be free of leading edge cavitation [31].

5.1.5. Mesh Independency

A converged and mesh independent solution is obtained when the result of the CFD simulation does not change with varying mesh fineness. As the runner is the main turbine component, it is important to check the mesh independency of the solution to have correct runner parameters such as the runner hydraulic efficiency.

There is a limit where the solution becomes mesh independent and the solution remains nearly constant but the computational effort drastically increases. As seen in Fig. 43 an approximately 2.5×10^5 mesh elements for one blade runner blade passage is acceptable to give accurate results for engineering purposes. Here $H_i - H_o$ is the head difference from runner inlet to runner outlet. So the mesh size is decided such that the solution is mesh independent and sufficient for optimization purposes, while keeping the computation time minimum.

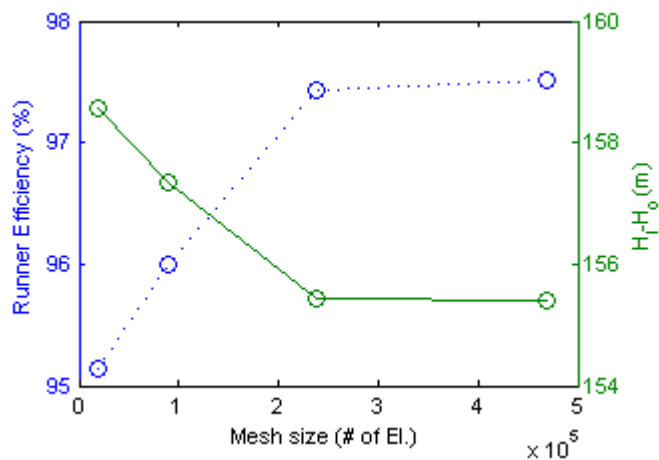


Figure 43. Runner efficiency and head difference versus number of mesh elements

5.1.6. Effect of Roughness on the Efficiency

During the optimization of the preliminary design the effect of the surface roughness is not taken into account. But since the manufacturing quality affects the roughness of the blade surfaces, the effect of roughness on the runner efficiency is investigated in the final design step for the sake of completeness. It is observed that the turbine efficiency drops 0.5 unit when the solid boundary condition is changed from “smooth” to a “roughness of 32 micron”.

5.1.7. Leakage Simulation and Check

Some of the design discharge is lost through the gap space between the runner and stationary parts. The leakage rate through the hub gap is calculated as $0.060 \text{ m}^3/s$, through the shroud gap as $0.035 \text{ m}^3/s$ according to the method proposed by Petermann [29]. In the CFD simulation, the expected inlet and outlet pressures are defined and the leakage rate is checked through the gap spaces. The pressure variation is plotted with the blade pressure contours in the same scale, the pressure contours are obtained are shown in Fig. 44. The net axial force on the runner outside surface is determined from this pressure distribution caused by the leakage flow. This force is transferred to structural design.

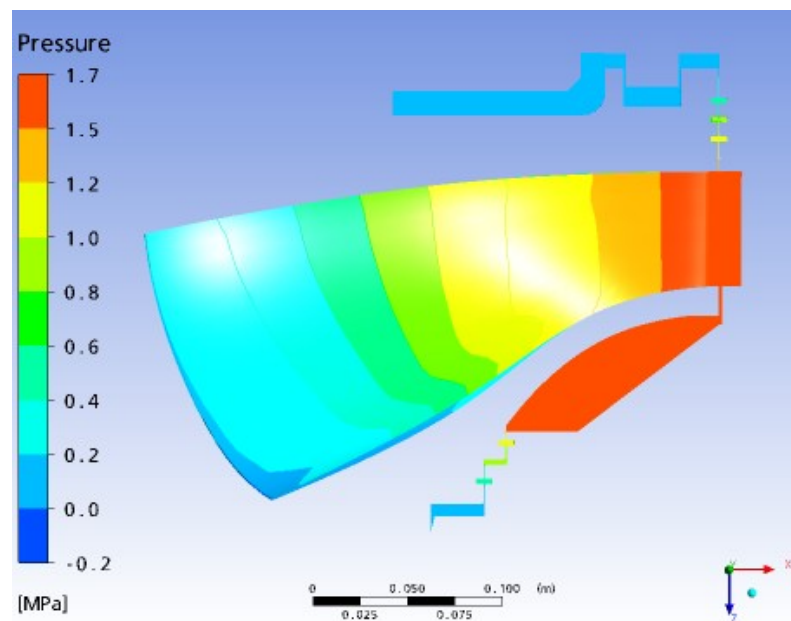


Figure 44. Simulated leakage domain plotted with runner blade

5.1.8. Final Blade Design

Final blade shape is obtained from Case 12 simulation. The parameters obtained from the CFD results are mentioned in Table 5.

A runner efficiency of 97.45 percent is obtained from the simulations, which satisfies the expectations, but lower than the maximum possible efficiency. Empirical volumetric and mechanical efficiency charts are presented by Kurokawa [37]. According to those empirical data, the overall runner efficiency is expected to be around 0.98 for a Francis turbine of specific speed $n_q = 32.5$. This indicates that either the runner efficiency is low; or that the best efficiency point of the turbine is slightly shifted.

The latter one is proved when the turbine runner is simulated with a lower discharge. When the same design is simulated in CFD, a runner efficiency up to 97.8% is reached at a %85 partial discharge operation.

It is possible to say that flow separation does not occur, because the meridional vectors follow the meridional paths as plotted in Fig. 45, and the pressure distribution supports this observation as shown in Fig. 46.

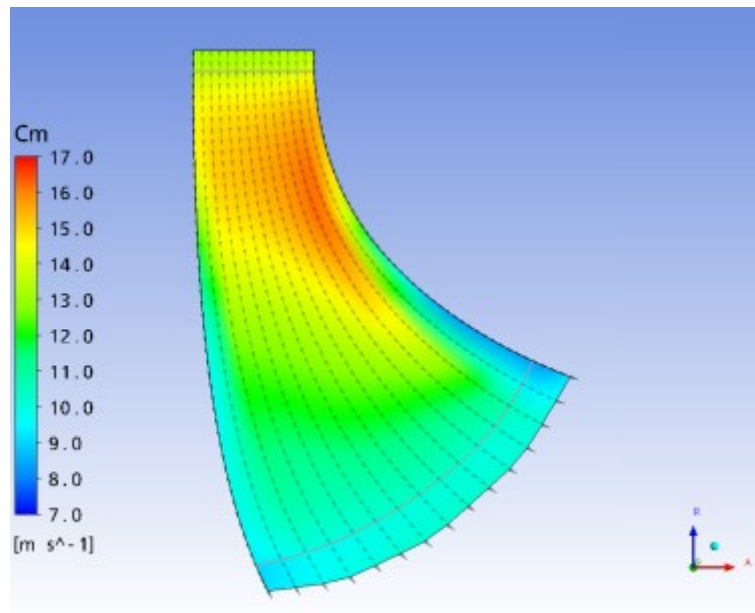


Figure 45. Meridional flow velocity vectors (Case 12)

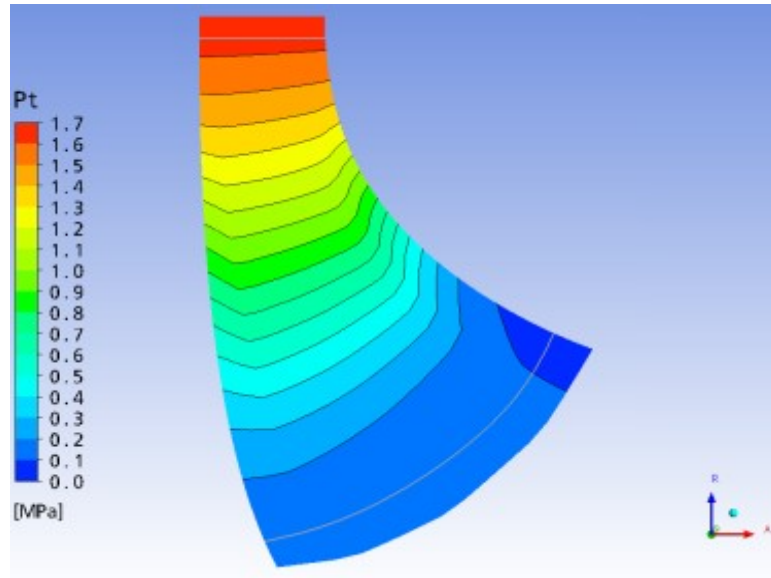


Figure 46. Variation of total pressure on meridional section (Case 12)

The velocity vectors shown in Fig. 47, follow the blade profile throughout the runner passage. Any flow separation on the blade is not expected in the meridional section from inlet to outlet.

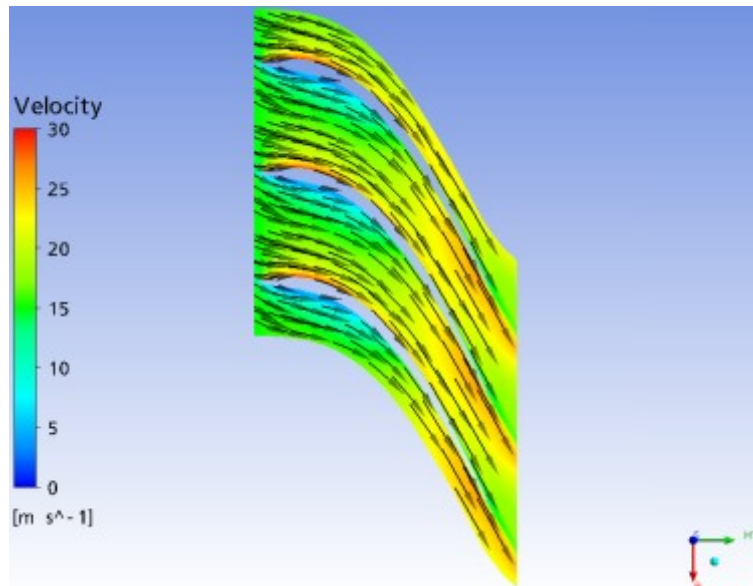


Figure 47. Velocity vectors for meridional section i3-03 (Case 12)

The same behaviour is valid for the meridional section close to the hub side as shown in Fig. 48, and the meridional section close to the shroud side shown in Fig. 49. For the same purpose the streamlines between the runner blades are examined as illustrated in Fig. 50.

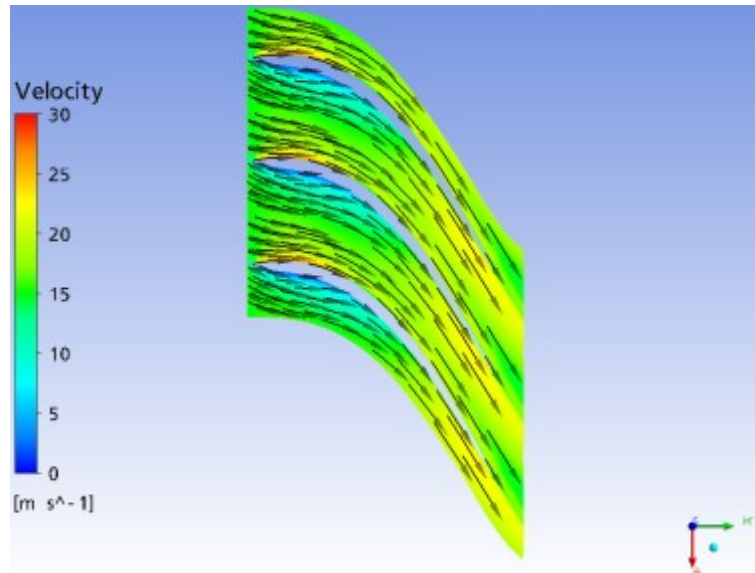


Figure 48. Velocity vectors for meridional section i4-o4 (Case 12)

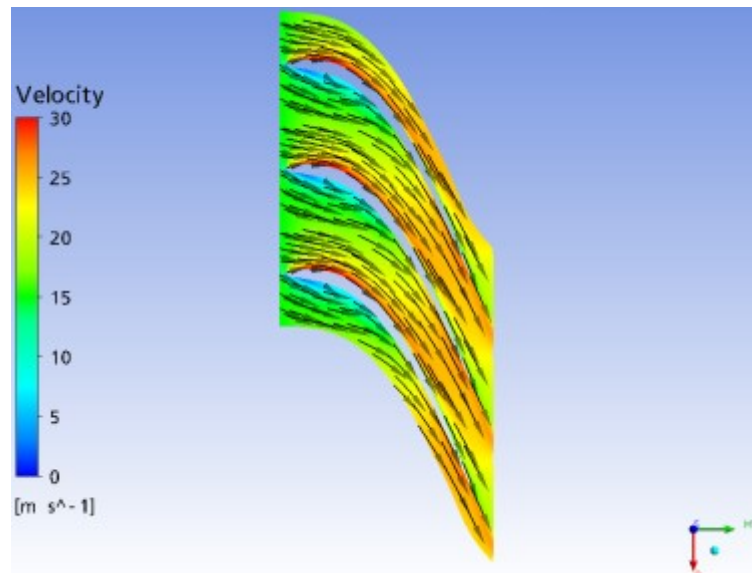


Figure 49. Velocity vectors for meridional section i2-o2 (Case 12)

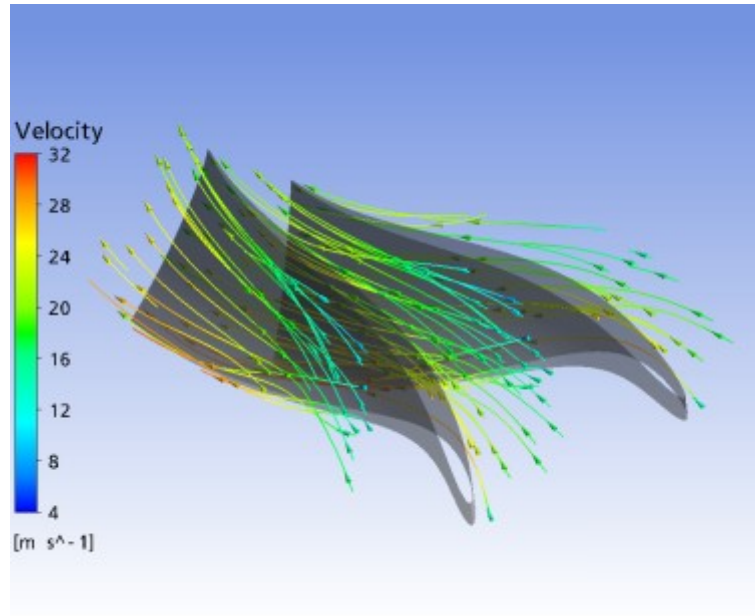


Figure 50. Velocity streamlines (Case 12)

5.2. Results for the Auxiliary Components

5.2.1. Spiral Case

For a balanced operation of the turbine, the equal distribution of the water around the runner is important. For this purpose the flow distribution is investigated by examining the ability of the spiral case to distribute the flow uniformly.

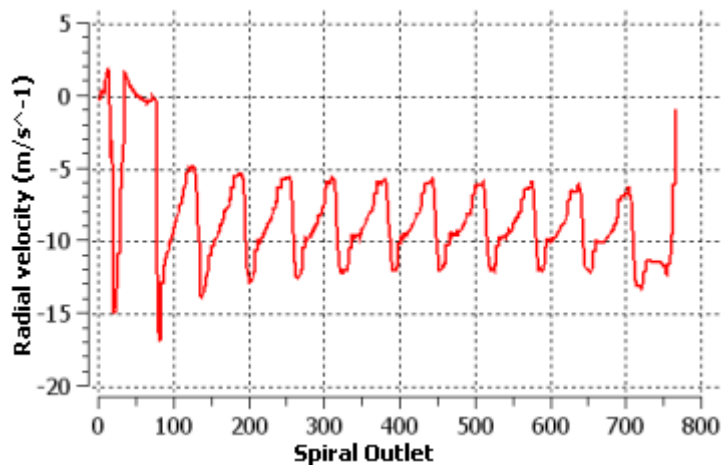


Figure 51. Radial velocity at the spiral case outlet

As plotted in Fig. 51, the radial flow velocity has a periodic distribution at the spiral outlet. The only exception is the end section which is connected to the spiral inlet section. The same behaviour is observed in the pressure and velocity distributions on the spiral mid-plane, shown in Fig. 52 and Fig. 53 respectively.

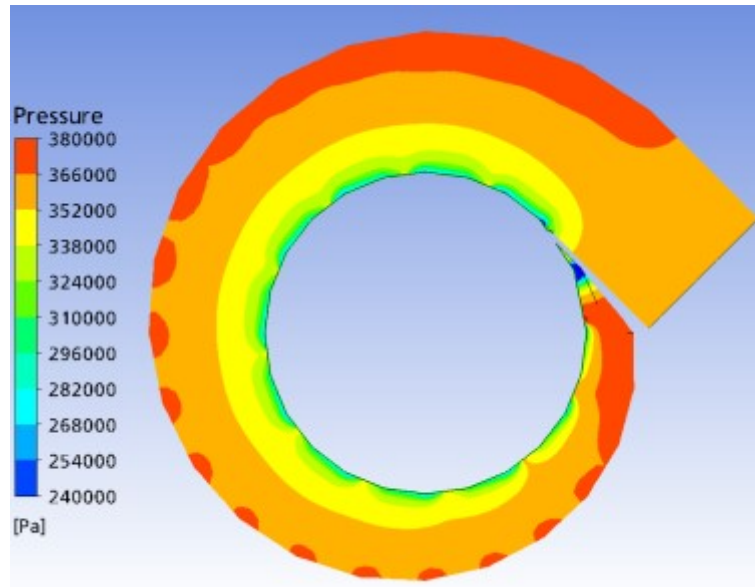


Figure 52. Pressure distribution on the spiral case mid-plane

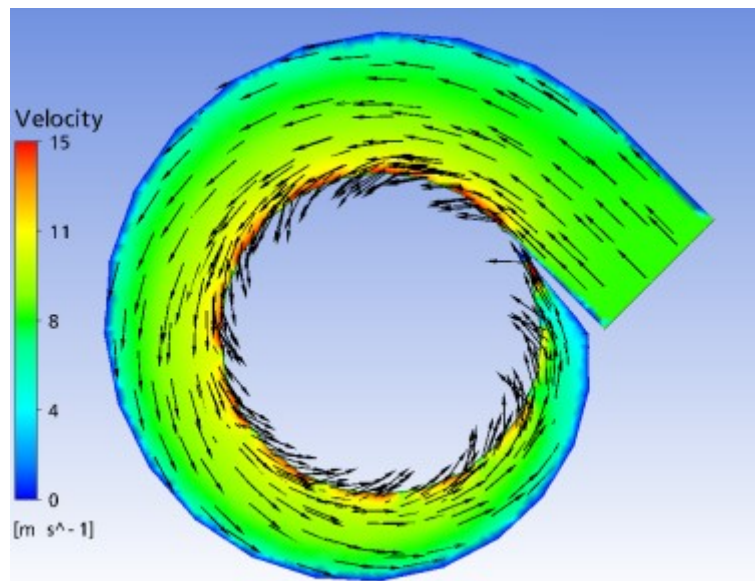
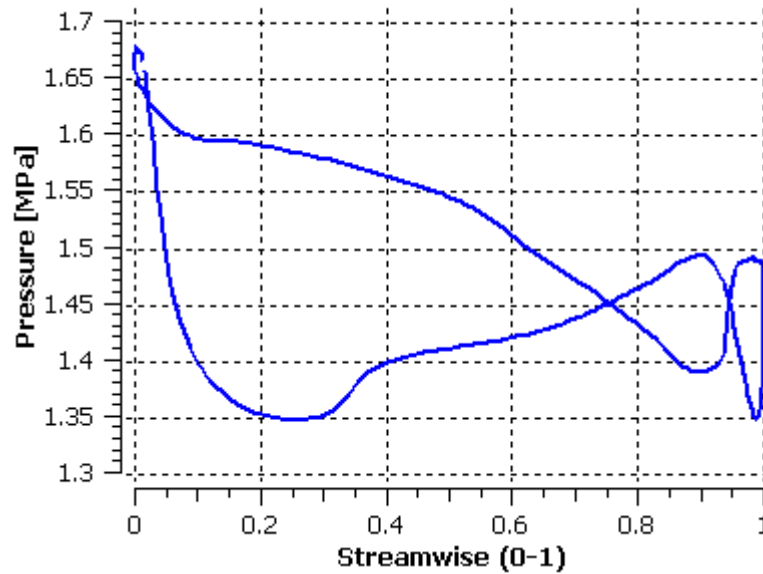


Figure 53. Velocity vectors on the spiral case mid section

5.2.2. Stay Vanes

The pressure distribution on the stay vane mid-section is obtained as in Fig. 54. According to the experience and literature survey, the stay vane loading distribution indicates a correct inflow and outflow angles of the stay vanes.



To observe the hydraulic losses, the average total pressures in the stay vane passage investigated. In Fig. 55, the total pressure contours are plotted on the meridional plane of stay vane passage. The averaged total pressure values at the stay vane inlet and outlet are compared for the determination of hydraulic losses at the stay vane cascade.

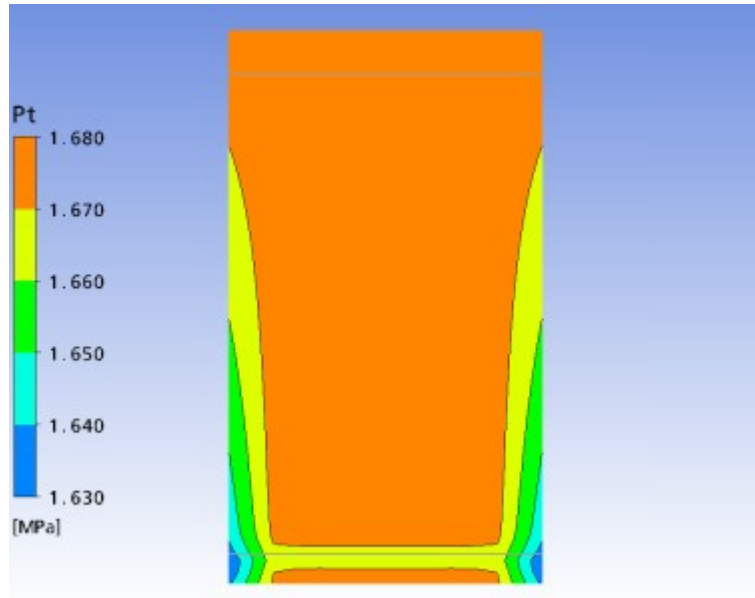


Figure 55. Distribution of total pressure on stay vane meridional section

Variation of the pressure (i.e the static pressure) in the stay vane passage is as shown in Fig. 56. The gradual pressure decrease between the stay vanes indicate again use of correct flow angles.

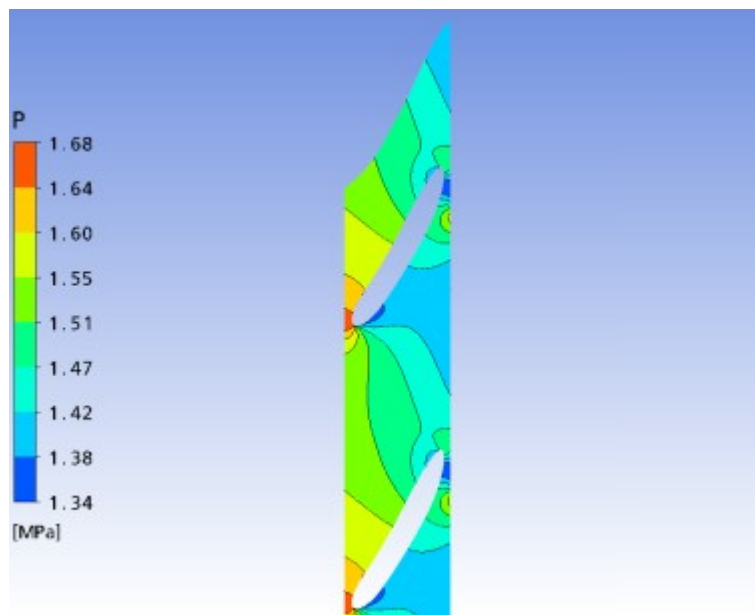


Figure 56. Distribution of pressure in the stay vane passage

As shown in Fig. 57, three dimensional velocity streamlines are also examined in order to demonstrate the uniformity of flow distribution between the stay vanes.

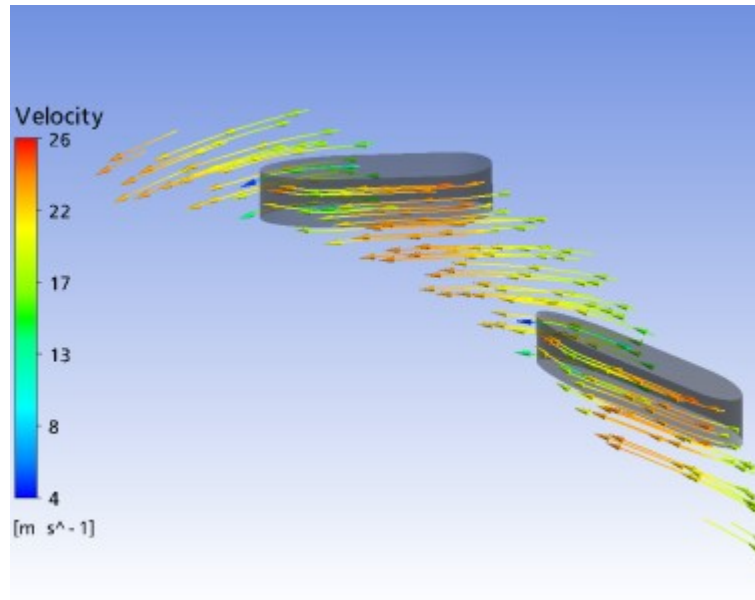


Figure 57. Velocity streamlines in the stay vane passage

Stay vanes are simulated with spiral case for the validation of the correct flow behaviour. The pressure distribution and flow vectors are plotted as shown in Fig. 58. This indicates an almost uniform distribution except the final smallest section of the spiral case. This change in one stay vane passage is not of major importance for the balanced operation of the runner.

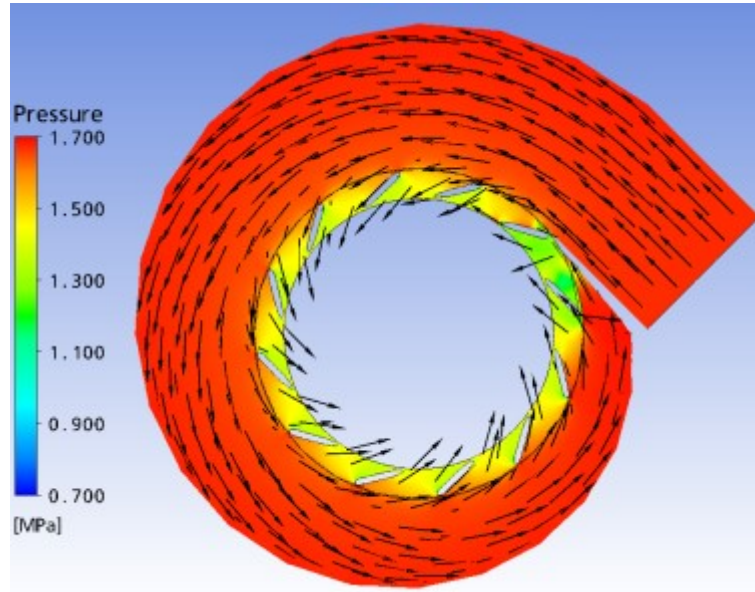


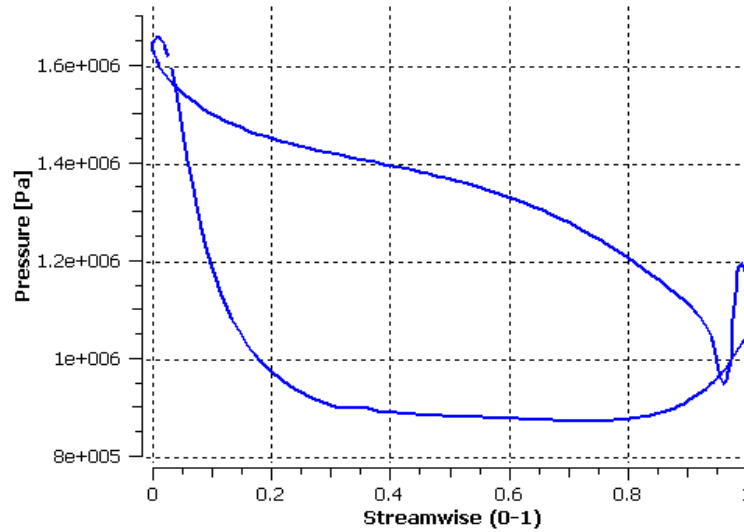
Figure 58. Pressure distribution and velocity vectors on the mid-plane of spiral case and stay vanes

5.2.3. Guide Vanes

NACA0024 airfoil profile is used to define the guide vane cross section. From the results of some previous CFD analysis of Francis turbine applications it is deduced that a symmetrical guide vane profile provides better flow behavior and pressure distribution behind the guide vane [22].

Guide vanes create wakes at the trailing edge. Enough space should be allowed between guide vane trailing edge and blade leading edge, in order to allow the mixing out of the wakes and prevent the wakes reaching the runner inlet. The minimum ratio of the guide vane trailing edge radius to the runner leading edge radius should be 1.04 to prevent the wakes reach the runner inlet. [33] [34]. In the final design of guide vanes this ratio is taken as 1.09.

The pressure distribution on the guide vane mid-section is obtained as in Fig. 59. According to the previous works, the guide vane loading distribution indicates a correct inflow and outflow angles of the stay vanes.



To determine the guide vane hydraulic losses, the average total pressures in the guide vane passage are investigated. In Fig. 60, the total pressure contours are plotted on the meridional plane of guide vane passage. The averaged total pressure values at the guide vane inlet and outlet are compared for the determination of hydraulic losses at the guide vane cascade.

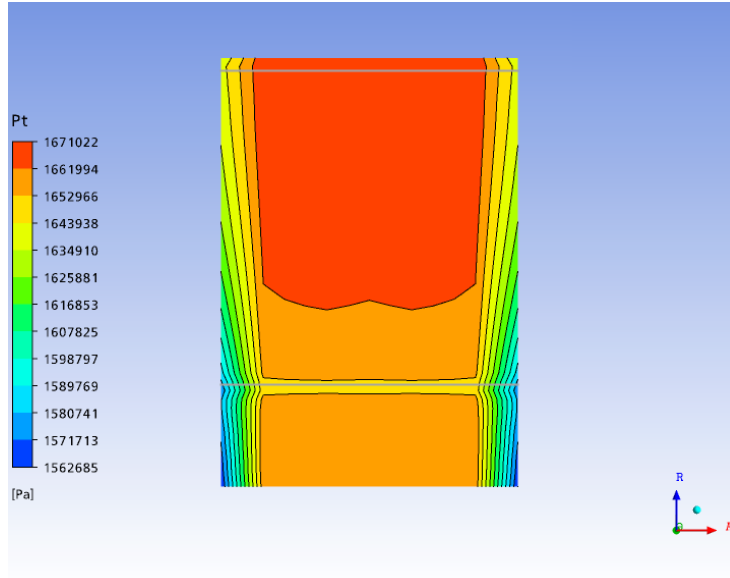


Figure 60. Distribution of total pressure on guide vane meridional section

Variation of the pressure (i.e the static pressure) in between the guide vanes is as shown in Fig. 61. The gradual pressure decrease between the guide vanes indicates again use of correct flow angles.

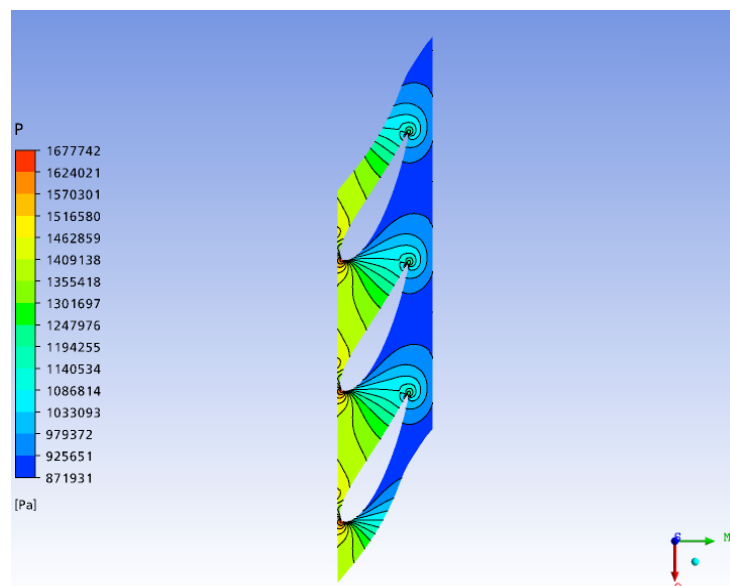


Figure 61. Distribution of pressure in guide vane passage

As shown in Fig. 62, three dimensional velocity streamlines are also examined in order to validate the flow distribution between the stay vanes.

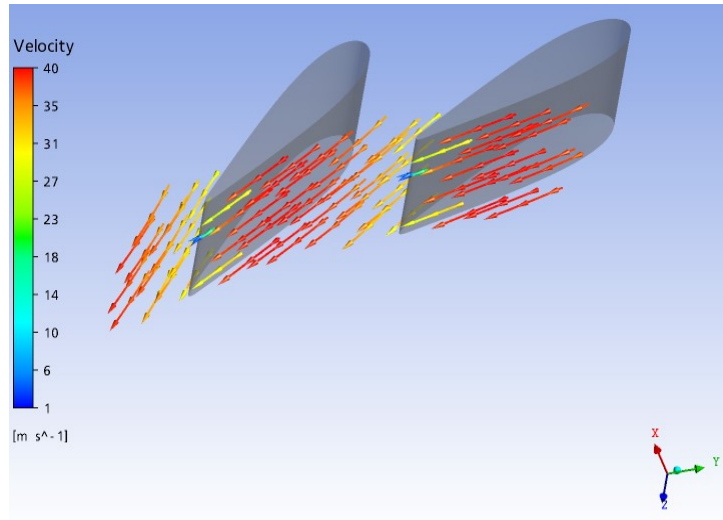


Figure 62. Velocity streamlines in guide vane passage

Guide vanes are also simulated with runner blades in order to check the flow angle match in between. The pressure variation and velocity vectors of this simulation with respect to the stationary frame of reference are shown in Fig. 63.

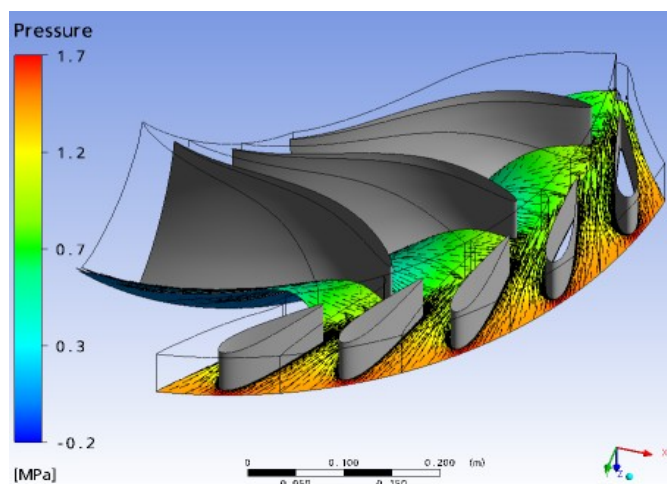


Figure 63. Simulation of guide vanes with runner blades

5.2.4. Draft Tube

The flow behaviour inside the draft tube is mainly investigated by plotting the velocity vectors and investigating the pressure recovery. From the average draft tube inlet and outlet velocities and pressures, the pressure recovery of the final draft tube design is calculated as 0.79, using the pressure recovery factor definition given in equation (45). The variation of the total pressure and the static pressure can be visualized in Fig. 64 and Fig. 65.

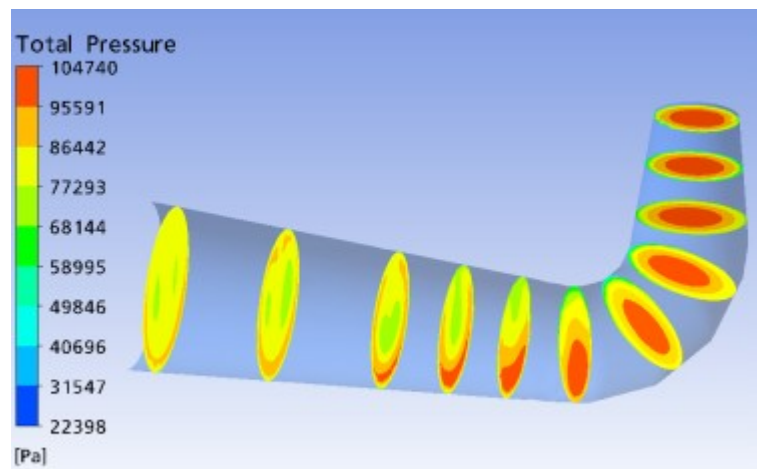
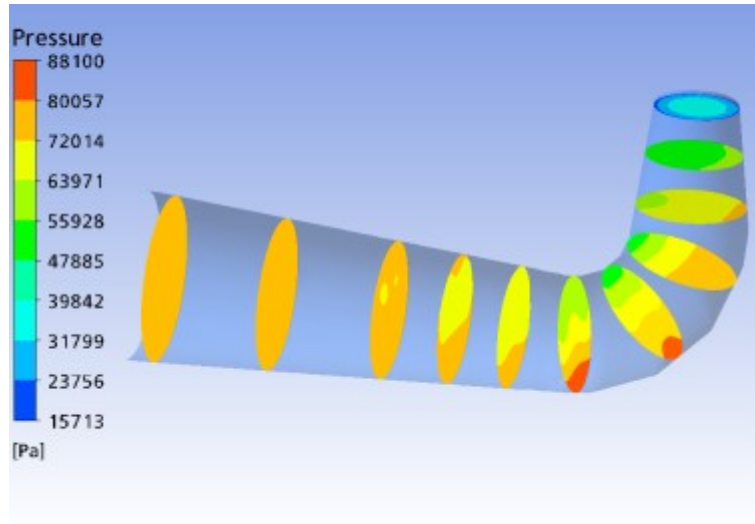


Figure 64. Change of total pressure through the draft tube

The total pressure decreases in the flow direction due to hydraulic losses, as shown in Fig. 64. The static pressure increases in the flow direction, which is the main role of the draft tube, as shown in Fig. 65.



The velocity vectors on the mid-section of the draft tube are plotted, as illustrated in Fig. 66: Any flow separation is not detected in the inlet cone of the draft tube according to Fig. 66 and the flow behaviour is as expected according to the streamlines plotted in Fig. 67.

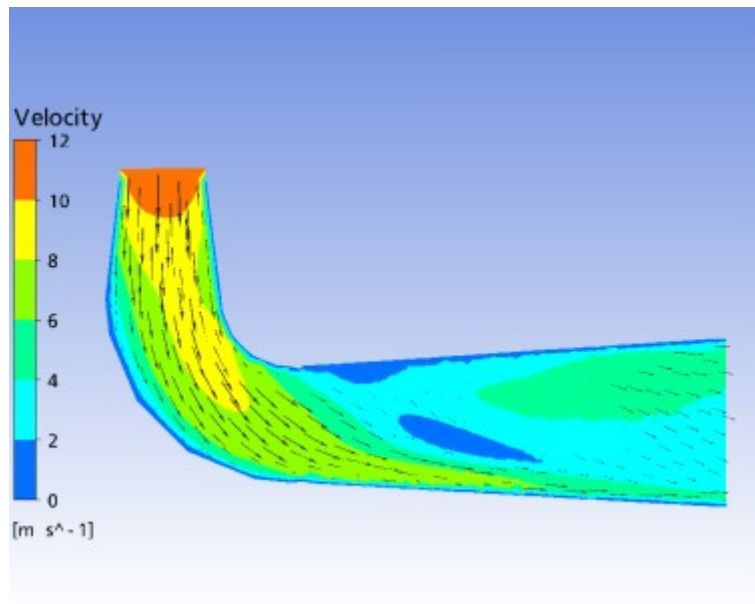


Figure 66. Velocity vectors on the draft tube mid-section

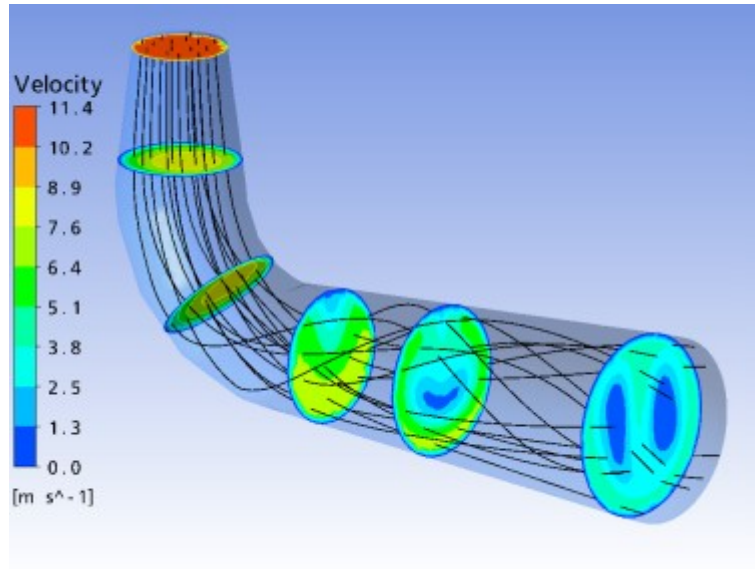


Figure 67. Velocity contours and streamlines in the draft tube

5.3. Hydraulic Losses and Summary of Final Results

The overall hydraulic efficiency of the components are calculated as presented in the following table:

Table 6. Summary of hydraulic losses

	Spiral	Stay vanes	Guide vanes	Runner	Leakage loss	Draft tube
Efficiency (%)	0.995	0.996	0.989	0.974		0.729
ΔH (m)	0.800	0.626	1.707	155.425	1.710	2.287
Overall efficiency (%)						0.944

5.4. Discussion of Results

The design discharge is $2 \text{ m}^3/\text{s}$ and the design head is 164.84 m . After passing the inlet valve, the flow enters the spiral case. Water is distributed around the stay vanes with a certain circumferential and radial velocity. For a balanced operation, the radial flow velocities are checked through the spiral outlet, as shown in Fig. 51. The pressure distribution at the spiral case outlet is found to be periodic as shown in Fig. 52. A safe operation of the spiral case is ensured, as the pressure distribution and flow velocity have periodic behaviour around the runner circumference. As shown in Table 6, 0.5% of the total energy is lost in the spiral case. This loss is equivalent to 0.80 m of head loss.

Water leaving the spiral case enters the stay vane cascade. The final design of stay vanes are actually decided according to its maximum structural strength, as mentioned in section 1.5 “Francis Turbine”. The stay vane profile and position is nevertheless dependent on its hydraulic performance: the hydraulic losses, inflow and outflow velocity angles are checked. As mentioned in Table 6, 0.4% of the hydraulic losses occur in stay vanes, leading to a head loss of 0.626 m. Stay vane behaviour with the spiral case is checked by a simulation of both components as shown in Fig. 58. The interaction of stay vanes with spiral case is found to be acceptable. The necessary stay vane outflow angle is decided upon the necessary guide vane inflow angle, given by the relation in equation (55), and the stay vane design is finalized.

Once the guide vane number and location are decided, the blade length can be computed according to equation (14). The guide vane profile is assigned according to the previous researches. Symmetric NACA profile is assigned as mentioned in the application chapter. The final guide vane design and guide vane orientation is obtained according to the CFD results. The optimum guide vane angle is calculated using equation (22) by implementing the conservation of momentum principle.

The final guide vane design is reached when the simulated guide vane flow angle matches the theoretical flow angle α_0 computed from equations (56) and (57). The hydraulic loss ratio of the final guide vane design is 1.1%, as shown in Table 6. A head of 1.707 m is therefore lost in the guide vane passage.

Once the theoretical inlet and outlet circulation values are computed in equations (36) and (37) respectively, the necessary inflow and outflow angles are computed. The runner blade model is then created by giving a profile defined in Fig. 34, and by assigning the blade angles δ illustrated in Fig. 13.

A series of simulations are performed in order to find the optimum blade geometry. In the first step, the overall geometry of the runner is optimized. The inlet and outlet diameters, hub and shroud profiles are modified to reach targeted efficiency and power values, as listed in Table 4. Once the required runner geometry is obtained, the blade LE and TE angles are adjusted. The theoretical inflow and outflow angles are derived from the definition of circulation and momentum given in equations (20) and (24) respectively. The blade angles are therefore adjusted with CFD, optimization test cases are listed in Table 5. The final design case is “Case 12” given in Table 5. To obtain a cavitation and shock-free design, the pressure distribution on the runner blade is examined. The leading edge shock is prevented, by the elimination of peak pressure at the inlet section comparing Case 9 and Case 10, shown in Fig. 37 and 38.

The final runner design has a hydraulic efficiency of 97.45 %. A head of 155.425 m is transformed to shaft rotation by the turbine runner, as mentioned in Table 6.

In the final design, the performance characteristics of the runner are calculated as 0.9404 for the head coefficient, and 0.3385 for the discharge coefficient, listed in Table 6. The head coefficient value is between 0.9 and 1.0, indicating a leading edge cavitation free operation and high efficiency at the design operation condition.

Vapor pressure in the design is calculated using equation (47). In the final design, Fig. 42 proves that the minimum pressure on the blade is held above the vapor pressure, preventing cavitation.

Even though the leakage loss is disregarded in the runner simulations, the computed leakage rate is checked with CFD simulations. The pressure distribution in the leakage domain is checked as shown in Fig.44. This pressure distribution enables the calculation of the net forces on the hub and shroud of the runner for structural check. As given in Table 6, a head drop of 1.71 *m* is observed due to leakage.

Once the turbine runner dimensions are decided, draft tube inlet dimensions are set accordingly. The geometry of the draft tube is decided upon the turbine orientation and power plant conditions. After the trial design cases, any flow separation in the inlet cone is prevented, as proved by Fig. 66.

The pressure recovery ability of the draft tube is investigated for the final design. The pressure recovery factor, computed from equation (45) , is found as 0.79 for this design. It is known that highly efficient draft tubes has recovery factors up to 0.90. The final design is however presumed to be efficient enough by examining the pressure distributions given in Fig. 64 and Fig. 65.

The performance of each turbine component is evaluated separately and listed in Table 6. According to the final CFD results, an overall turbine efficiency of 94.4% is reached. This high efficiency is however reflects the efficiency of the turbine in ideal geometric and manufacturing conditions. More rough surfaces than expected would cause an efficiency drop, as mentioned in the application chapter.

This hydropower project is a new medium scale hydropower plant named Cuniş HPP. The hydropower station is being constructed in the Black Sea region of Turkey. All the design and manufacturing, including the electromechanical equipment, are handled in Turkey. Hence this project is unique to be constituted

completely by Turkish investments, Turkish designers and manufacturers. The design of the turbines is undertaken by the groups of designers working at private company Su-Ener. The generator design and manufacturing are undertaken by TEMSAN, Turkish Electromechanics Industry. All the parts of the Francis turbines are being manufactured in either one of the factories of TEMSAN located at Diyarbakır and Ankara, with the collaboration of other Turkish producers, in Ostim Ankara, and material providers in many other cities in Turkey.

The academic research included in this thesis work covers the application of analysis tools, such as CFD, and investigation of the results. The complete research is not limited to hydraulics but includes also structural verification and solid modeling in civil engineering and mechanical engineering areas. Several research papers have been published either on national or international conferences, about the structural design [43], parametric solid modeling [44], CFD design [45],[46] and design optimization methodology [10] of hydraulic turbines.

The manufacturing is accomplished according to the provided drawings. The manufactured pieces are controlled according to the restrictions and allowances permitted by the hydraulic design and structural design, indicated as on the drawings. Samples pictures showing the solid model and manufactured components are presented in Appendix A. .

CHAPTER 6

CONCLUSION

6.1. Summary of the Developed Work

A design and optimization methodology is developed for the hydraulic design of a Francis turbine using computational fluid dynamics tools. The net head and the design discharge of the system are the only inputs to start the process. In the preliminary stage, the hydraulic machinery theory and some empirical equations are used for overall dimensioning of the turbine.

The preliminary design is improved by using a commercial CFD tool which is known as validated by intensive academic and industrial applications. CFD results enabled inspection of local problems on the turbine elements and curing by iterative correction. The design is optimized to increase turbine efficiency while satisfying the hydraulic performance factors which differ for each turbine component. The pressure and velocity distributions are checked for spiral case and stay vanes. For guide vane and runner, the computed flow angles are considered as indicators of performance. The pressure recovery is investigated for the draft tube. Cavitation zones are eliminated by iterative CFD solutions for improved geometries.

The developed methodology is applied for the turbine design of an actual hydropower project. The project is a medium scale hydropower plant named Cuniş HPP located in the Black Sea region of Turkey. A Francis turbine with a power of

2.94 MW is designed. CFD results indicated an overall turbine efficiency of 94%. The turbine will be in operation in 2010-2011 period. Complete design and manufacturing including the electromechanical equipment are accomplished in Turkey. Hence, this project is unique to be constituted completely by Turkish investors, designers and manufacturers.

6.2. Contributions of the Developed Work

A turbine design know-how is developed using state-of-the art modeling tools, for the first time in Turkey. The design methodology, coupled with structural and solid modeling tools, enables the turbine design ready for manufacturing. This work is the part of an actual hydropower project in realization stage. The work is an outcome of the successful collaboration between the academia and the industry.

The thesis work covers the development of the Matlab codes to accelerate the iterative design process involving extensive CFD applications. Once the structural safety is validated, the solid model is created according to the final optimized design.

Achievement of a turbine design know-how is expected to create a positive impact on the development of hydropower industry in the country scale, including production of all electromechanical equipment involved in a hydropower plant. As the manufacturing is performed in Turkey, this study will also have a contribution on the procurement of qualified workers in the turbine manufacturing area and attract new investments in the hydropower industry.

6.3. Future Work

The procedure described in the thesis can be extended for transient investigations using CFD tools which require larger computing capacity. Unsteady simulations

covering the rotor-stator interactions, draft tube vortices can be investigated in order to improve the turbine design. Future works may also consist of the application of the design methodology to other types of turbines.

REFERENCES

- [1] *The Large Dams Debate*, World Commission on Dams, <http://www.dams.org/about/debate.htm> (accessed 08/03/10).
- [2] Kaygusuz, K., Sari, A. (2003). “*Renewable energy potential and utilization in Turkey.*” *Energy Conversion and Management*, 44 (3), pp.459-478.
- [3] *Hydroelectricity Consumption*, World Energy Council Turkish National Committee, <http://www.dektmk.org.tr/incele.php?id=MTA2> (accessed 08/15/10)
- [4] Devlet Su İşleri Genel Müdürlüğü <http://www.dsi.gov.tr/kurumsal/tarihce.htm> (accessed 08/15/10)
- [5] *Türkiye Enerji Raporu 2009*, Dünya Enerji Konseyi Türk Milli Komitesi, 0013/2009, Ankara.
- [6] Parkinson, E. (1995). “*Test Case 8: Francis Turbine.*” Turbomachinery Workshop Ercoftac II, IMHEF, EPFL, Lauzanne.
- [7] Sottas G., Ryhming I.L. (1993). “*3-D Computation of Incompressible Internal Flows.*” *Proceedings of the GAMM Workshop, Notes Numerical Fluid Mechanics (NNFM) 39*, Vieweg Verlag, Braunschweig.

- [8] Roth, S., Calmon, F., Farhat, M., Muench, C., Huebner, B., Avellan, F. (2009). “*Hydrodynamic Damping Identification from an Impulse Response of a Vibrating Blade.*” 3rd IAHR International Meeting of the Workgroup on Cavitation and Dynamic Problems in Hydraulic Machinery and Systems, October 14-16, 2009, Brno, Czech Republic.
- [9] Nicolet, C., Arpe, J., and Avellan, F. (2004). “*Identification and modeling of pressure fluctuations of a Francis turbine scale model at part load operation.*” Proceedings of the 22nd IAHR Symposium on Hydraulic Machinery and Systems, Stockholm, Sweden..
- [10] Celebioglu, K., Okyay, G., Yildiz, M. (2010). “*Design of a Francis Turbine for a Small Hydro Power Project in Turkey.*” Proceedings of ASME 10th Biennial Conference on Engineering Systems Design and Analysis (ESDA 2010), July 12-14, 2010, Istanbul, Turkey.
- [11] *Hydroelectric Power Generation*, Environment Canada,
<http://www.ec.gc.ca/eau-water/default.asp?lang=En&n=BCC55AC6-1#hydro>
(accessed 08/08/10)
- [12] *Hydroelectricity*, Wikipedia The Free Encyclopedia,
<http://en.wikipedia.org/wiki/Hydroelectricity>
(accessed 08/08/10)
- [13] Raabe, J. (1985). “*Hydropower: The Design, Use, and Function of Hydromechanical, Hydraulic, and Electrical Equipment.*” VDI-Verlag, Verlag des Vereins Deutscher Ingenieure, Düsseldorf.
- [14] Dixon, S. L. (1998). “*Fluid mechanics and thermodynamics of turbomachinery.*” Elsevier, USA.

- [15] Fluid machinery lecture notes
http://nptel.iitm.ac.in/courses/Webcourse-contents/IIT-KANPUR/machine/ui/Course_home-lec28.htm (accessed 08/08/10)
- [16] Keck, H., Drtina, P., Sick, M. (1996). "Numerical Hill Chart Prediction by Means of CFD Stage Simulation for a Complete Francis Turbine." Proceedings of the XVIII IAHR Symposium, Valencia.
- [17] Keller, M. (2006). "CFD of Unsteady Phenomena in Water Turbines" 24th CADFEM User's Meeting.
- [18] Keck, H., Sick, M. (2009). "Thirty Years of Numerical Flow Simulation in Hydraulic Turbomachines." Acta Mechanica, 201, pp.21-229.
- [19] Launder, B.E., Spalding, D.B. (1972). "Mathematical Models of Turbulence." Academic Press, London, New York.
- [20] Roache, P.J. (1972). "Computational Fluid Dynamics." Hermosa Publishers, Albuquerque, New Mexico.
- [21] Suzuki, T., et al. (1996). "Flow Behaviour around Stayvanes and Guidevanes of a Francis Turbine". ASME Journal of Fluids Engineering, 118, pp.110-115.
- [22] Wu, J., et al. (2007). "CFD-Based Design Optimization for Hydro Turbines". ASME Journal of Fluids Engineering, 129, pp.159-168.
- [23] Muntean, S., et al. (2010). "Numerical Analysis of the Flow in the Old Francis Runner in Order to Define the Refurbishment Strategy." U.P.B. Scientific Bulletin, Series D, 72(1), pp.117-124.

- [24] Harano, M. Tani, K, Nomoto, S. (2006). "*Practical Application of High-performance Francis-turbine Runner Fitted with Splitter Blades at Ontake and Shinkurobegawa No.3 Power Stations of the Kansai Electric Power Co. Inc.*" Hitachi Review, 55(3), pp.109-113.
- [25] *Guide on How to Develop a Small Hydropower Plant*, European Small Hydropower Association – ESHA, 2004.
- [26] Krivchenko, G.I. (1986). "*Hydraulic Machines: Turbines and Pumps*". Mir Publishers, Moscow.
- [27] *International Standard on Hydraulic turbines, storage pumps and pump-turbines – Model acceptance tests*, IEC 60193:1999(E).
- [28] Finnemore, E.J., Franzini, J.B. (2002). "*Fluid Mechanics with Engineering Applications*". 10 ed., McGraw Hill, pp.707.
- [29] Petermann, H. (1978). "*Akım Makinaları*". Matbaa Teknisyenleri Basımevi, Istanbul.
- [30] Busea, C., Jianu, S. (2004). "Optimization of Axial Hydraulic Turbines Runner Blades Using Hydrodynamic Simulation Techniques". Scientific Bulletin of the Politechnica University of Timisoara, Transaction on Mechanics Special Issue, HMH 2004, Romania, pp.67-72.
- [31] Avellan, F. (2004). "*Introduction to Cavitation in Hydraulic Machinery*" Scientific Bulletin of the Politechnica University of Timisoara Transactions on Mechanics Special Issue, HMH 2004, Romania, pp.11-22.
- [32] Milos, T., Barglazan, M. (2004). "*CAD Technique Used To Optimize The Francis Runner Design*". Scientific Bulletin of the Politechnica University of Timisoara, HMH 2004, Timisoara, Romania, pp. 125-130.

- [33] Jansen, W. (1964). “*The Design and Performance Analysis of Radial-inflow Turbines*”. NREC Report, 1067-1.
- [34] Maki, H., Mori, Y. (1973). “*On the Study of the Flow Through an Impeller of Mixed and Inward Flow Radial Turbines*”. Bull JSME, 16(91), pp.81-92.
- [35] Muntean, S., Susan-Resiga, R., Anton, I. (2002). “*3D Flow Analysis of the GMM Francis Turbine for Variable Discharge*”. Proceedings of the Hydraulic Machinery Systems 21st IAHR Symposium, Lausanne.
- [36] Goto, A., et al. (2002). “*Hydrodynamic Design System for Pumps Based on 3D CAD, CFD, and Inverse Design Method*”. Journal of Fluids Engineering, 124, pp. 329-335.
- [37] Kurokawa, J., Kitahora, T. (1994). “*Accurate Determination of Volumetric and Mechanical Efficiencies and Leakage Behavior of Francis Turbines and Francis Pump – Turbine*”. XVII IAHR Symposium, Beijing, China, pp.889-900.
- [38] Nennemann, B., Vu, T. C., Farhat, M. (2005). “*CFD prediction of unsteady wicket gate-runner interaction in Francis turbines: A new standard hydraulic design procedure*”. HYDRO 2005 International Conference and Exhibition, Villach, Austria, 17-20 October 2005.
- [39] Susan-Resiga, R., et al. (2006). “*Jet Control of the Draft Tube Vortex Rope in Francis Turbines at Partial Discharge*”. 23rd IAHR Symposium – Yokohama October 2006.
- [40] Drtina, P., Sallaberger, M. (1999). “*Hydraulic turbines—basic principles and state-of-the art computational fluid dynamics applications*”. Proceedings of the Institution of Mechanical Engineers, 213(C), pp.85-102.

- [41] Oh, H. W., Yoon, E. S. (2007). “*Application of computational fluid dynamics to performance analysis of a Francis hydraulic turbine*”. Proceedings of the Institution of Mechanical Engineers, Journal of Power and Energy, 221 (A4), pp. 583-590.
- [42] Ansys CFX, Release 11.0, User Manual
- [43] Chen, W., Celebioglu, K. (2009). “*Structural Analysis of a Francis Turbine Using Finite Elements Method*”, Proceedings of Nuclear & Renewable Energy Resources Conference 2009, September 28-29, Ankara, Turkey, pp.378-383.
- [44] Yildiz, M., Celebioglu, K. (2009). “*Parametric Modeling of a Francis Turbine*” Proceedings of Nuclear & Renewable Energy Resources Conference 2009, September 28-29, Ankara, Turkey, pp.402-407.
- [45] Okyay, G., Celebioglu, K., Aydin, I., Ger, M. (2009). “*Design of a Francis Type Water Turbine Using Computational Fluid Dynamics Methods*”, Proceedings of Nuclear & Renewable Energy Resources Conference 2009, September 28-29, Ankara, Turkey, pp.388-394.
- [46] Okyay, G., Celebioglu, K., Aydin, I., Ger, M. (2009). “*Design of a Francis Type Water Turbine Using Computational Fluid Dynamics Methods*”, International Journal of Electrical Energy Systems, Special Issue 2009 (1)1, pp.71-75.

APPENDIX A

SAMPLE PICTURES OF TURBINE PARTS

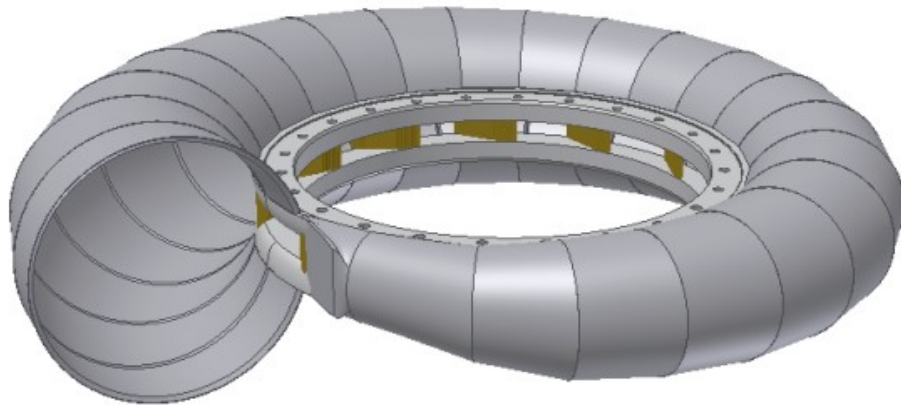


Figure 68. Spiral case solid model modeled after CFD simulations

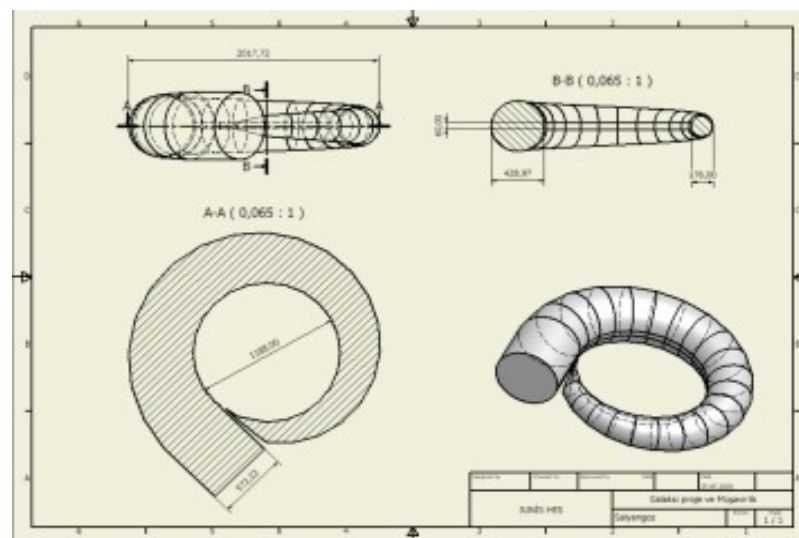


Figure 69. Sample drawing for spiral case



Figure 70. Manufactured spiral case according to final design



Figure 71. Manufactured turbine runner according to CFD design

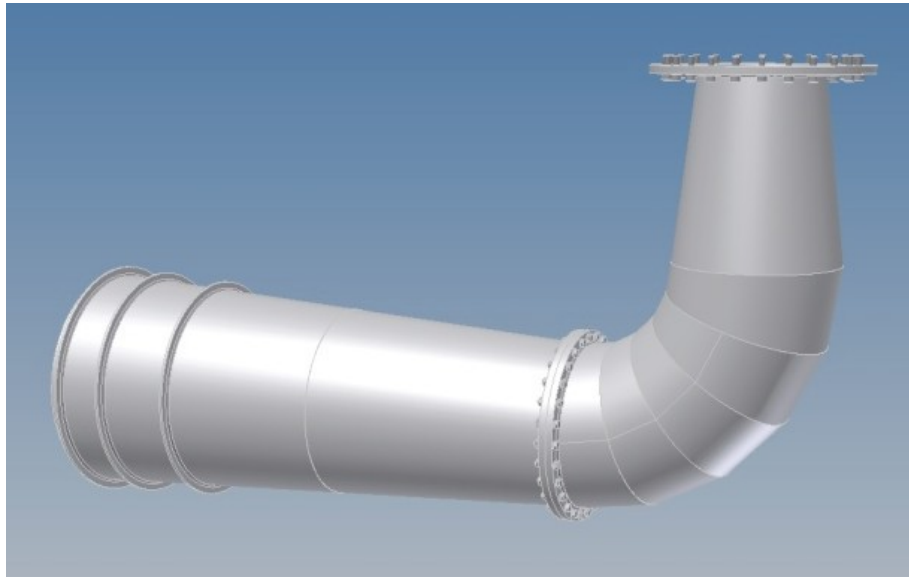


Figure 72. Solid model of the draft tube according to CFD design



Figure 73. Manufactured draft tube parts according to final design